Exploring RhoBAST Aptamer-Dye Complexes for Enhanced Metabolite Sensing

Megan Stein

Defense Date:

April 3, 2024

University of Colorado Boulder

Department of Biochemistry

Spring 2024

Thesis Advisor: Dr. Amy Palmer (Department of Biochemistry)

Committee Members: Dr. Halil Aydin (Department of Biochemistry),

Dr. Nancy Guild (Department of Molecular Cellular & Developmental Biology)

Table of Contents

Abstract

RNA is an essential component of cellular processes from gene expression to protein formation. A biosensor is a tool that turns binding of a metabolite of interest into a fluorescence signal. This project aims to explore and optimize RNA-based biosensors by comparing the binding affinity and fluorescence intensity between a previously researched RhoBAST-MaP555 aptamer-dye complex and other forms of rhodamine dyes. By evaluating the fluorescence output of JFX 549-Halotag and JF 549-alkyne, I aim to broaden the dyes that can be used in a RhoBAST complex. In future work this should increase the ability to track multiple metabolites with biosensors. The structural differences in deuterated JFX 549-Halotag and JF 549-alkyne, compared to MaP555 will lead to more insight on the structural necessities when it comes to the RhoBAST-dye complex. This thesis is a systematic examination of the steps necessary to acquire RhoBAST DNA, purified RNA, and Fluorescence Assays with reflections on my research experience as a whole.

Introduction

The History of Biosensors

The inception of biosensors represents one of the most creative inventions of our time. From food control to biomedical research, biosensors are pivotal devices that have led to an abundance of discoveries. The "father of biosensors" Leland C. Clark, Jr. created one of the first applicable biosensors, an electrode system, which detected oxygen in the blood in 1956 paving the way to the present day where over 84,000 biosensor reports have been produced (Bhalla et al., 2016; Clark & Lyons, 1962).

Biosensors are made up of a number of key components, including the analyte, bioreceptor, transducer, and the output/electronics/display as presented in Figure 1. These components come together to measure reactions in which the signal detected is proportional to the concentration of the substance being measured. These substances are known as analytes. Once the analyte is detected by the bioreceptor the transducer converts the energy produced into a measurable output signal. The electronics prepare the transducer's signal and display the results in the units of the analyte (Bhalla et al., 2016).

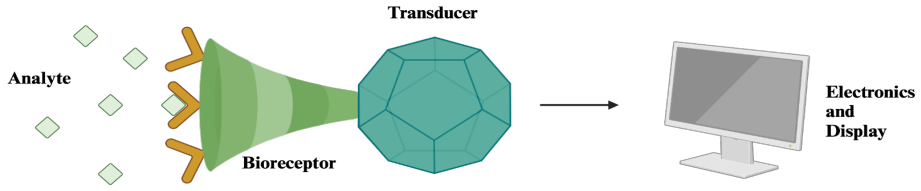

Figure 1: Representative image of a biosensor with the signal moving from left to right. A bioreceptor can be cells, DNA, enzymes, or aptamers which specifically recognize the analyte of interest. The Transducer converts energy into different read-outs based on the analyte-bioreceptor interaction. The read-out can be a variety of signals such as pH, photo diode, etc. Lastly there is the electronics/display which processes transducer signals and quantifies the results which are then displayed in numbers, wavelength, etc. Adapted from (Bhalla et al., 2016). Created with Biorender.com

While these pieces of the puzzle are important, there are also certain parameters that must be met in order for a biosensor to be effective and accurate. Selectivity of the biosensor is important to ensure the analyte being measuring is the one of interest. A relevant example of selectivity is the interaction between a ligand and a bacterial phenol sensor. These sensors use selectivity filters/checkpoints which screen the ligands entering the pathway based on size and chemical features, ensuring the ligand of interest proceeds to the binding pocket (Sahil et al., 2023)**.** It is also important for a sensor to have high reproducibility. A biosensor is not a reliable tool if it gives different results for the same experiment. Next are stability and sensitivity. A biosensor with stability ensures outside disturbances cannot easily alter the signal of the sensor, and the sensitivity of a sensor determines the minimum amount of analyte present that can be detected, giving a strong bottom baseline. Lastly a biosensor should have a linear detection range meaning as the concentration of analyte is increased or decreased, the signal response is linear over the allowable detection range.

While physical biosensor devices have their importance in the field, the majority measure analytes in samples such as blood, urine, water, and soil, i.e. specimens that are outside of an organism or a cell. However, it is also possible to place biosensors inside of cells. Intracellular biosensors have the same overall design features as a physical biosensor. They contain a sensing domain that binds the analyte of interest, a transducer domain so that the binding event is communicated to the final domain that has a read out in the form of fluorescence, luminescence, or colorimetric change. Intracellular biosensors have revolutionized biochemistry by allowing researchers to study molecules and biochemical reactions in live mammalian cells. The rest of this introduction will focus on features that are important for intracellular biosensors.

Fluorescence

Biosensors are only useful if we can visualize the analyte of interest. This is where fluorescence becomes crucial to the conversation**.** What makes fluorescence so powerful is that it is very sensitive (Lichtman & Conchello, 2005). Fluorescence is the light emitted after the absorption of a photon (at a specific wavelength) giving the exact amount of energy needed to transition outer orbital electrons from the low-energy ground state (S_0) to the first excited state, S_1. Once the energy threshold is reached, absorption occurs which excites the electron to S_1. Immediately after excitation, some energy is lost due to vibrational relaxation. The excited electron must eventually return to the ground state by either non-radiative or radiative decay. Radiative decay is the process of fluorescence, where the molecule emits a photon as the electron returns to the ground state. It is also possible for the electron to undergo intersystem crossing and convert to the triplet state and then decay by phosphorescence back to the ground state. Finally, non-radiative decay is the loss of energy due to heat, collisions, or molecular motion. These electronic transitions are depicted in Figure 2a (Herman, 1998; Lichtman & Conchello, 2005). Because of the loss of energy due to vibrational relaxation, the energy of the emitted light is always lower in energy (higher in wavelength) than the absorbed light (Figure 2b).

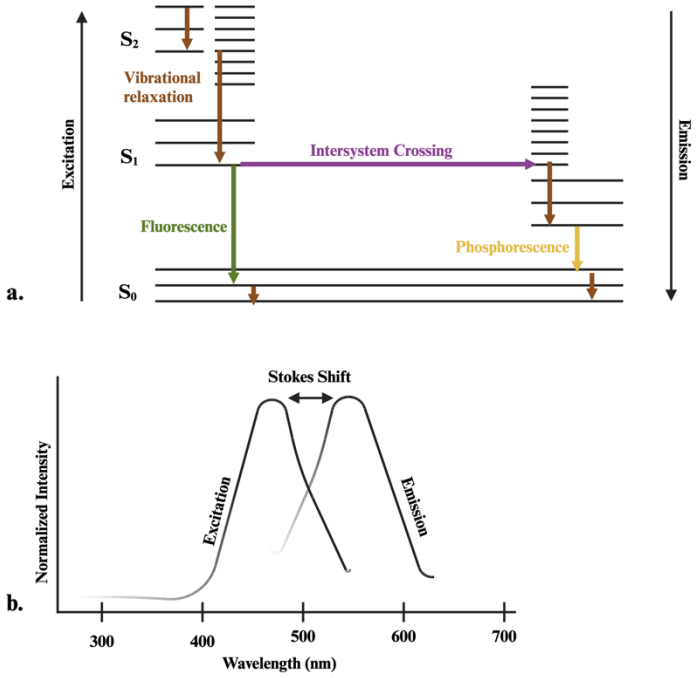

Figure 2: Fluorescence (a) A visual representation of a Jablonski diagram which shows the energy transitions from the ground state to the excited state. Intersystem crossing is another form of energy conversion (similar to vibrational relaxation) in which there is a forbidden transition (spin flip) to the triplet state vs. the singlet state (Lichtman & Conchello, 2005). (b) Generalized figure showing an excitation and emission spectrum of a fluorophore which exhibits symmetry and a difference in peak wavelengths otherwise known as Stokes shift. Created with BioRender.com

Fluorescent probes, otherwise known as fluorophores, are molecules which are capable of emitting light after absorbing a photon. Small molecule fluorophores have a low-molecular weight and wide range of chemical and photophysical properties (Martynov et al., 2016). For a molecule to fluoresce, it must contain conjugated double bond systems which allow the electron density to be delocalized over the molecule. If there are more conjugated double bonds in a molecule then the energy difference between the ground state and excited state becomes smaller. With a smaller energy difference between states, a lower-energy photon is able to excite the outer electrons into the excited state (Lichtman & Conchello, 2005). More conjugated pi bonds in an aromatic system can also give rise to a higher fluorescence quantum yield which is a

measure of fluorescence efficiency. The quantum yield is defined as the number of photons emitted divided by number of photons absorbed; a perfect fluorophore would have a quantum yield of 1. The molar extinction coefficient (ε) defines how well a fluorophore absorbs light at a particular wavelength, the higher the molar extinction coefficient the better molecule absorbs energy. A high extinction coefficient (high propensity to absorb light) and a high quantum yield (high propensity to emit light) will make for a bright fluorophore. Another feature of fluorophores is the planarity of the molecule and whether there are bonds capable of rotation. One advantage of a planar conjugated pi system is that the molecule has less vibrational degrees of freedom which allows for more energy to be emitted as a photon leading to a higher quantum yield. These molecules also tend to have higher photostability, while nonplanar fluorophores with rotatable bonds have more vibrational motion leaving them less photostable.

To characterize fluorophores, we collect an excitation and emission spectrum. These spectra show different intensities of light absorption and fluorescence at varying wavelengths, with the emission peak shifted toward longer wavelengths (Figure 2a). The excitation spectrum is measured by placing the detector at a specific emission wavelength and scanning the incident light that contributes to fluorescence emission at the defined wavelength. This process measures what absorbing species contribute to emission at that particular wavelength. An excitation spectrum is very similar to an absorption spectrum. The emission spectrum is measured by exciting the fluorophore at its excitation peak and measuring the emitted light as a function of wavelength. As mentioned before, the emitted light is lower energy (longer wavelength) than the light absorbed which causes a wavelength shift in the emission peak. This is known as the Stokes shift and varies in fluorophores (Figure 2b). A fluorophore with a wide emission spectrum will

often overlap with another fluorophore causing signal bleed-through, so fluorophores with narrower spectra are preferred.

There are many features of fluorescence that make it ideal for visualizing biological events that one could not see with the naked eye. Fluorophores become even more powerful when they are used in biosensors to detect changes in specific molecules and biochemical reactions.

Fluorescent Protein Biosensors

Fluorescent protein biosensors are an abundantly engineered form of biosensors with the ability to track analytes or biochemical reactions in living cells (Greenwald et al., 2018). These sensors have been designed for a wide range of cellular metabolites, ions, and enzymatic reactions. As the name suggests, these biosensors rely on the use of fluorescent proteins (FPs) as the fluorophores. Green fluorescent protein (GFP) was originally discovered in the *Aequorea victoria* jellyfish; it immediately revolutionized biology due to the protein being intrinsically fluorescent as a result of a formation of the chromophore (p-hydroxybenzylidene-imidazolidone) when the protein folds (Tsien et al., 1998). Scientists further discovered they could mutate the protein to engineer the fluorescent properties, including color, brightness, and photostability. Fluorescent proteins are especially important in the engineering of biosensors. The majority of FP-based biosensors utilize Förster Resonance Energy Transfer (FRET) as the read-out. These FRET-based biosensors are made by fusing two fluorescent proteins that are different colors and have overlap between the emission of the donor FP and absorption of the acceptor FP to a sensing domain (Bajar et al., 2016). The general concept of a FRET-based biosensor is illustrated

in Figure 3. Binding of the analyte to the sensing domain changes the conformation of the sensor, bringing the donor and acceptor FP close together, thus increasing the efficiency of FRET.

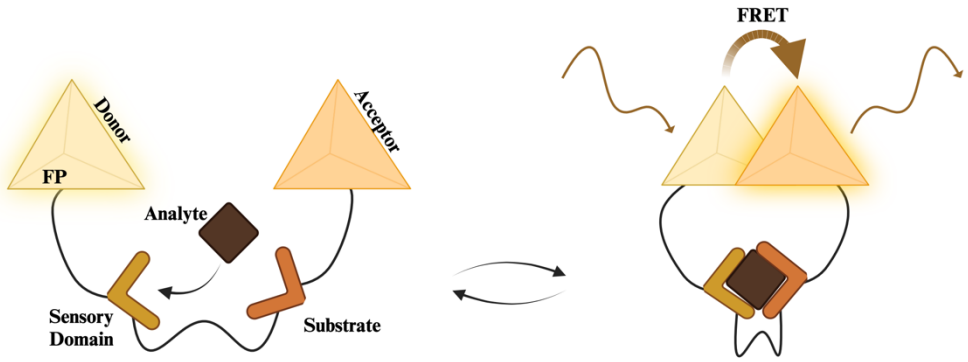

Figure 3: Representative image of a Förster resonance energy transfer (FRET) intramolecular sensor. Once the analyte binds the sensory domain, a conformational change is induced in the sensor and the donor and the acceptor come into a FRET proximal distance leading to a change in the FRET signal (Bajar et al., 2016). Created with Biorender.com

While protein biosensors have opened up the possibility of tracking molecules and ions in living cells, there are limitations with fluorescent protein sensors that cannot be ignored. There are over 800 fluorescent protein biosensors, most of which use the same FPs (cyan fluorescent protein and yellow fluorescent protein) preventing simultaneous FRET sensor use for different analytes (Greenwald et al., 2018). FP's have relatively wide spectra which can lead to bleed through due to the extensive overlap with other fluorescent proteins (Ovechkina et al., 2021). Finally, FPs tend to have a lower quantum yield than small molecule fluorophores and they tend to be more susceptible to photobleaching which prevents the fluorophore from fluorescing and makes it harder to visualize metabolites over long periods of time.

Fluorescent proteins are a pivotal part of science and imaging, but what if there was a way to optimize signal, intensity, and measure multiple metabolites using a broad range of colors? Luckily scientists have started to explore making biosensors out of RNA and small molecule fluorophores.

RNA-based Biosensors

Ribonucleic acid (RNA) is a single stranded molecule composed of a phosphate backbone and the sugar ribose. Similarly to DNA, RNA contains nitrogenous bases: adenine (A), cytosine (C), guanine (G) and instead of thymine (T), RNA contains Uracil (U). DNA can be replicated and transcribed into RNA which can then be further translated into proteins. Although many textbooks depict RNA as single stranded and unstructured, in reality RNA contains hydrogen bond base pairings and base stacking which allow RNAs to fold into a complex secondary structure. This folding can result in a tertiary structure which creates a binding pocket, allowing for the recognition of small molecules (Wang D et al., 2024). RNA folds naturally and efficiently under physiological conditions, such as a temperature of 37 °C, a pH around 7.4 and low ionic concentrations (Leamy et al., 2017). RNA also has the ability to recognize and bind small molecules due to an evolutionary advancement called riboswitches which regulate gene expression in microorganisms. Riboswitches are RNA elements that bind cellular ligands, such as metabolites. Riboswitches contain two distinct domains, one for specific small molecule binding and the other for generating a genetic regulatory signal (Baird et al., 2010). Once the ligand is bound to the ligand-binding domain, the riboswitch undergoes a conformational change that then transforms the RNA into a genetic regulatory element. This is a major component of downstream translation initiation control and transcription in microorganisms.

A perfect example of efficient and specific riboswitches are bacterial riboswitches which regulate transcription (Figure 4).

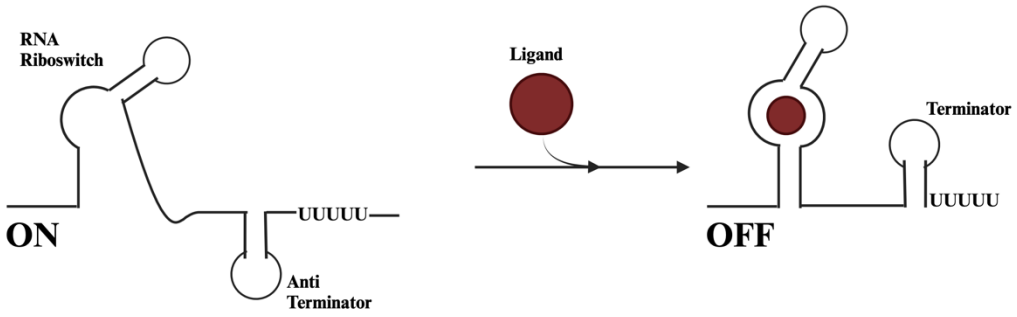

Figure 4: A visual representation of a bacterial riboswitch regulating transcription. The short-stemmed loop structure (riboswitch) contains an anti-terminator and when ligand-free is allowing DNA to be transcribed into RNA. Ligand binding promotes formation of the termination hairpin riboswitch causing transcription to end prematurely.

The folding efficiency and natural selectivity for small molecules make RNA the perfect candidate for a fluorescent biosensor. An RNA-based biosensor consists of four different modules which contribute to overall fluorescence. There is the aptamer, also known as the receptor module, the communication module, the fluorogenic module and finally the cellular stabilization module. Binding of the analyte to the aptamer module leads to communication of the binding event via allostery to the fluorophore binding module, which leads to folding of the fluorophore binding module. This allows the fluorophore to bind and turn on fluorescence (Figure 5) (Bhalla et al., 2016).

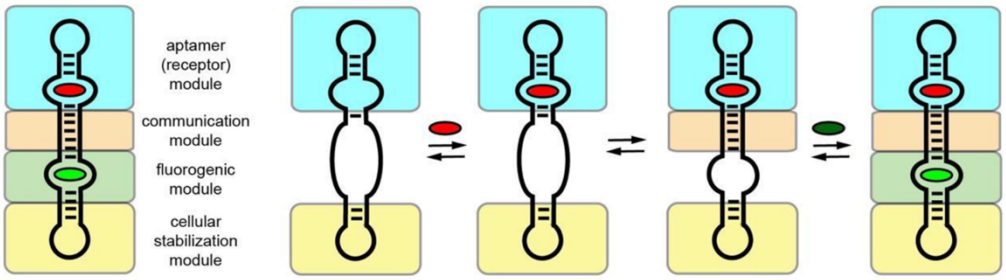

Figure 5: Schematic of an RNA-based biosensor and the four modules that make it up. Once the analyte binds to the aptamer, the binding event is communicated to the fluorescence module, enabling the fluorophore to bind and turn on fluorescence. Adapted from Rob Batey. Created with Biorender.com

One of the first engineered fluorophore-binding aptamers is Spinach. Spinach was engineered to bind 3,5-difluoro-4-hydroxybenzylidene imidazolinone (DFHBI), a green

fluorophore (Paige et al., 2012). Spinach was attached to a small molecule-binding aptamer through a communication module to create the first RNA-based biosensor. This first RNA-based biosensor was designed for S-adenosyl methionine (SAM) which is a crucial molecule in one carbon metabolism, a pathway that is often perturbed in cancer. SAM is the primary methyl donor in biology and is important for DNA and RNA methylation and amino acid metabolism. In bacteria, the SAM riboswitch regulates genes involved in cysteine and methionine biosynthesis. The SAM-Spinach RNA-based biosensor relies on the binding of SAM to the sensing domain (the SAM-III riboswitch) which stabilizes the communication module and induces a conformational change in the Spinach aptamer which allows fluorophore binding (McDaniel et al., 2003). While Spinach folds well *in vitro*, it exhibits poor folding *in vivo* making it a sub-optimal tool for real-time measurements of cellular SAM concentrations. This poor folding of Spinach led to the development of a new aptamer Squash. Squash was evolved to bind to 1,8-diazafluoren-9-one (DFHO) from naturally an occurring adenine riboswitch which had robust folding (Dey et al., 2022). Squash was incorporated into the SAM biosensor in place of Spinach. However, while Squash can exhibit high levels of folding, the small molecule dyes that Squash binds, DFHO and DFHBI, have very broad excitation and emission spectra due to rotational mobility. For example, in Figure 6, the excitation and emission spectra of DFHO are compared to another dye, tetramethylrhodamine (TMR). This Figure shows that DFHO has a much wider spectra in comparison. The broad excitation and emission spectra make it difficult to multiplex Squash/DFHO with other fluorophores.

The Spinach-SAM and Squash-SAM biosensors showed that RNA can be used to build fluorescent biosensors. But the photophysical properties of the dyes used were suboptimal. Photophysics is one of the most important aspects when designing fluorogenic RNA-aptamers.

The aptamer should be bright (high quantum yield and extinction coefficient), photostable (maintains fluorescence upon repeated illumination), and have narrow excitation and emission spectra (to enable multiplexing). This is where we land on the need for an RNA-aptamer that has efficient folding and robust photophysics.

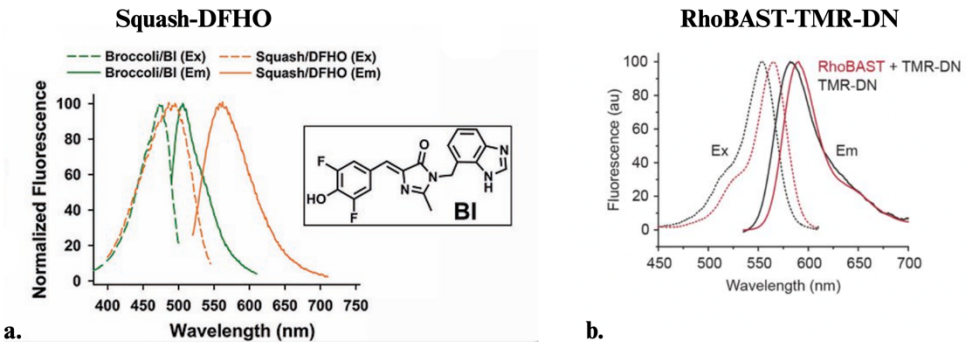

Figure 6: Excitation and emission spectra of RNA/fluorophore aptamers. (a) Excitation and emission spectra of the Squash-DFHO aptamer-dye complex. Also included is another aptamer, Broccoli. Image adapted from (Dey et al., 2022). (b) Excitation and emission spectra of RhoBAST-TMR-DN complex. Image Adapted from (Sunbul et al., 2020). This figure is to show the comparison in spectra between the complexes. Squash-DFHO is noticeably broader than the RhoBAST-TMR-DN complex, leaving this complex more susceptible to photobleaching and bleed through.

The Rhodamine Binding Aptamer for Super-resolution imaging Techniques (RhoBAST) is an aptamer that was evolved to bind fluorogenic rhodamine dyes (Sunbul et al., 2021). This aptamer was selected to bind tetramethylrhodamine-dinitroaniline (TMR-DN). Dinitroaniline is a fluorescence quencher; when TMR binds the RhoBAST aptamer, the DN quencher is separated from the TMR fluorophore, and the fluorescence turns on. The RhoBAST aptamer complexed with TMR-DN retained 90% of the fluorescence at 0.25 mM of magnesium which suggests it will work effectively under physiological conditions. MaP555 is another rhodamine dye that can bind to RhoBAST and fluoresce (Figure 7). The RhoBAST-dye complex is based on fast-ligand exchange which prevents photobleaching from causing any issues when imaging. MaP555 remains in a closed lactone state when unbound to an aptamer, but when binding to an aptamer or in this case RhoBAST it induces a shift of the dye into an open lactone state which allows

fluorescence (Figure 7). RhoBAST is a multi-faceted aptamer readily available to engineer, modify, and place into a biosensor.

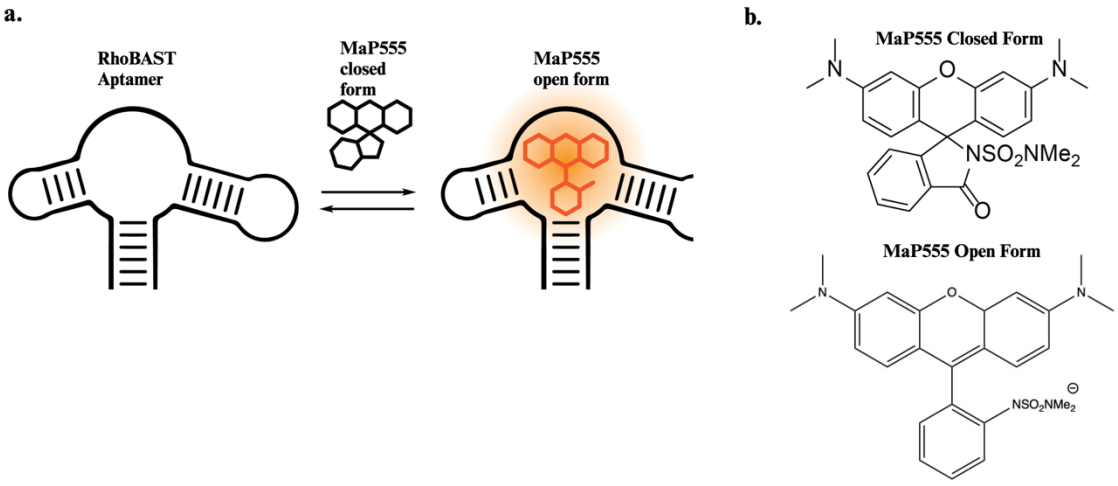

Figure 7: Schematic the RhoBAST aptamer binding to MaP555. (a) The RhoBAST aptamer binds the closed form of MaP555 which causes a ring opening to occur on MaP555. The ring opening initiates fluorescence turn-on. Image adapted from (Englert et al., 2023). (a) Structure of MaP555 dye in closed and open form. Created with BioRender.com.

Research Objective

The RhoBAST aptamer inspired the Palmer and Batey labs to look closer at the aptamer-dye complex and design a sensor platform using RhoBAST as the fluorogenic RNA in biosensors with different sensing modules for a diverse array of metabolite sensors. While the aptamer is important, the dyes that can pair with the aptamer are equally crucial to the application of this fluorogenic module into sensors. Why have one dye when you can use multiple and tailor them to the need of the molecule and obtain maximum florescence?

The primary focus of this project was to compare the binding affinity and fluorescence properties of an already reported RhoBAST-MaP555 complex to other RhoBAST-dye complexes. The dyes I chose were Janelia Flour (JF) X 549-Halo tag and Janelia Flour (JF) 549-Alkyne (Figure 8). Both JF dyes are rhodamine-based dyes which contain an equilibrium between lipophilic colorless lactone and the fluorescent zwitterion ion (Figure 8a) (Zheng et al.,

2019). The equilibrium between the lactone and zwitterion is represented by an equilibrium constant (K_{L-Z}), where a K_{L-Z} greater than 1 means the zwitterion is favored and a K_{L-Z} less than 1 means the lactone is favored. JF 549 has a high K_{L-Z} (3.47) which means the dye is in the zwitterionic open or fluorescent form even when not bound to RNA. These dyes also have a high molar extinction coefficient (101,000 $M^{-1}cm^{-1}$) and quantum yield of 0.88 (Grimm et al., 2020).

In my thesis project I sought to compare RhoBAST bound to JF dyes to the MaP555 complex. I also wanted to compare structural differences between two dyes with the same absorbance and see how that would affect the binding affinity. Janelia Flour (JF) X 549-Halo-tag contains a Halo-tag ligand (chloroalkane) at a specific position in the molecule. The Halo-tag ligand is a chloroalkane functional group (Figure 8b) that reacts with the Halo-tag enzyme. The "D" indicates that instead of hydrogens on the azetidine rings of the xanthene core, there are deuterium atoms. These deuterium atoms can significantly increase the fluorescence efficiency, the brightness of the dye, and inhibit photobleaching, overall improving the photophysical properties of the dye (Grimm et al., 2021). Comparing the deuterated and Halo-tag ligand JF 549 dye to a JF 549 with an alkyne functional group can provide insight to the binding patterns of RhoBAST and perhaps identify new dyes that could be used in RhoBAST-based biosensors.

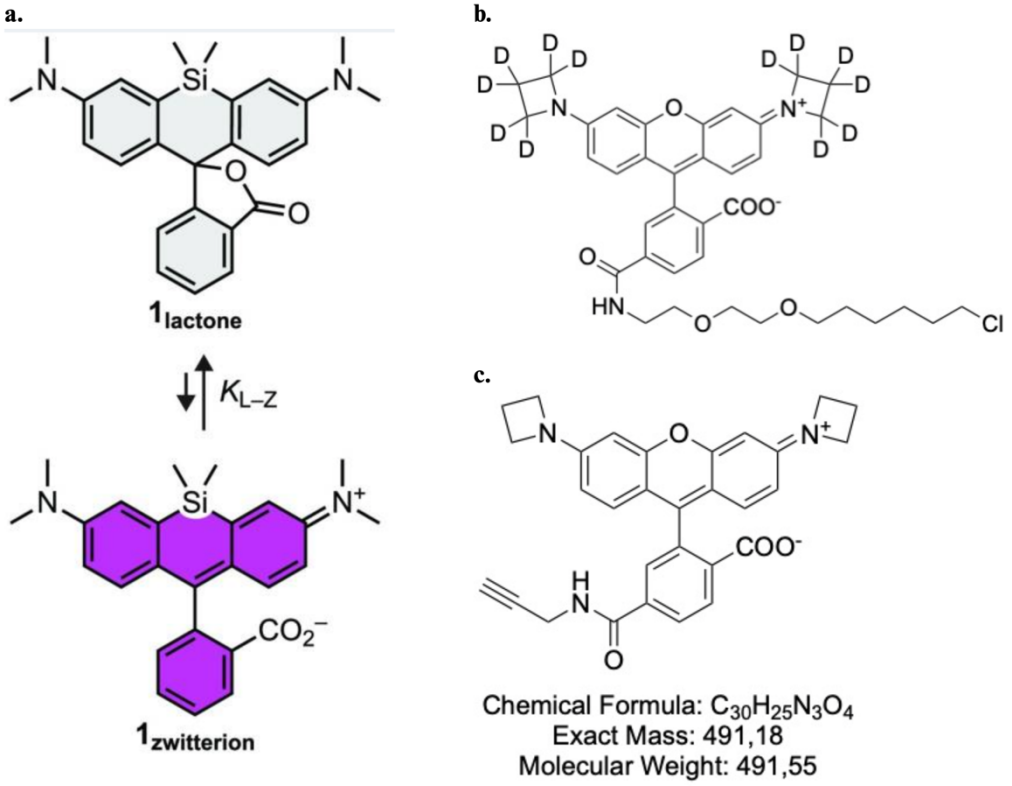

Figure 8: (a) Structural representation of the lactone fluorescent zwitterion ion equilibrium adapted from (Zheng et al., 2019) (b) Structural representation of JFX 549-Halotag with the deuterated functional groups which are added in both NR_2 positions replacing the hydrogens. (c) Structural image of JF 549-Alkyne.

Method and Materials

Table 1: Reagents Table

	Reagents	Designation	Source
	Diethylpyrocarbonate (DEPC) Treated Water 0.1%	Reagent	Created in the Palmer Lab
PCR:			
	PFU DNA Polymerase Buffer	Reagent	Agilent #600153-82
	10 mM deoxynucleotide triphosphate (dNTPs)	Reagent	New England Biolab
5'- GGA ACC TGA GGC GGT TAA – 3'	100 mM 3' RhoBAST primer	Primer	Integrated DNA Technologies (IDT)
5' – GGG ACG GTA GAC TAC CGC TTA GAG AGTTTA CGG -3'	100 nM 3' Squash primer	Primer	Integrated DNA Technologies (IDT)
5' - GAA TTC TAA TAC GAC TCA CTA TAG GGA CGG TAG GCT ACA AGG TGA GCC CAA TAA TAC GG -3'	100 nM 5' Squash Primer	Primer	Integrated DNA Technologies (IDT)
5' – GGT CCA TCC CGA ATC CGC TTA GAG AGT TTA CGG CTC TAC TTC CTA TCC TAA CCC AAA CGC TAT TAT TGG GCT CAC CTT GAT TCC CTT TCG GTT ACA AGG CAT CTG GAC C – 3'	Antisense Squash strand 1:100 dilution of 100 µM	Template	Integrated DNA Technologies (IDT)
5'- GCG CTA ATA CGA CTC ACT ATA GGG ACG GAA CCT CCG CGA AAG C- 3'	100 mM 5' RhoBAST Primer	Primer	Integrated DNA Technologies (IDT)
5'- GGA ACC TCC GCG AAA GCG GTG AAG GAG AGG CGC AAG GTT AAC GCG CTC AGG TTC - 3'	Antisense RhoBAST strand 1:100 dilution of 100 µM	Template	Integrated DNA Technologies (IDT)
	10x PFU DNA Polymerase	Enzyme	Agilent #600353
PCR Check Gel:			
	Agarose	Reagent	Sigma Aldrich
	1x Tris base, acetic acid, EDTA buffer (TAE)	Reagent	Created in the Palmer Lab

	Ethidium bromide	Reagent	Sigma Aldrich
	NEB 6x gel loading dye	Dye	New England Biolabs #B7024A
	1 kb plus DNA ladder	Reagent	New England Biolabs #N3233S
***In vitro* Transcription:**			
	10x Transcription buffer: 400mM Tris (pH 8.0) 100mM DTT 20mM spermidine 0.1% Triton X-100	buffer	Created in the Batey Lab
	2M Magnesium Chloride	Reagent	Sigma Aldrich
	1M Dithiothreitol (DTT)	Reagent	Created in the Batey Lab
	100 mM ATP 100 mM CTP 100 mM GTP 100 mM UTP	Reagent	A26209-1G C1506-1G G8877-1G U3750-1G
	T7 RNA Polymerase	Enzyme	Created in the Batey Lab
	Inorganic pyrophosphate (IPP)	Enzyme	Created in the Batey Lab
Polyacrylamide Page Gels/RNA Purification:			
	Tetramethylethylenediamine (TEMED)	Reagent	Sigma Aldrich
	10% Ammonium Persulfate (APS)	Oxidizing Agent	Thermofisher
	Diluent (8M Urea & 1x TBE)	Reagent	Created in the Palmer Lab
	20% Acrylamide (8M Urea & 1x TBE)	Reagent	Created in the Palmer Lab
	Tris-borate-EDTA (TBE)	Reagent	Created in the Palmer Lab
	Formaldehyde loading dye 11:20	Dye	Created in the Palmer Lab
	Tris-EDTA (TE)	Reagent	Created in the Palmer Lab
Fluorescent Plate Assays/ Dye Characterization:			
	10x Adaptive buffer sizing (ABS): 3M KCl 1M $MgCl_2$ 1M HEPES-NaOH	Buffer	Created in the Palmer Lab
	Map555	Dye	Spirochrome
	JFX 549-Halotag	Dye	Lavis Lab
	JF 549-Alkyne	Dye	Lavis Lab
	Dimethyl sulfoxide (DMSO)	Reagent	472301-100ML Sigma-Aldrich
	Ethanol-Trifluoracetic acid (ETOH-TFA)	Reagent	Created in the Palmer Lab

Polymerase Chain Reaction (PCR)

The goal of a PCR experiment is to amplify a specific DNA fragment, in my case the fragment was the RhoBAST aptamer. The DNA fragment of interest contained the aptamer itself with a T7 tail (5' – TAATACGACTCACTATAG – 3') for *in vitro* transcription and a G-C clamp (5' – GCG CGC – 3') to ensure specific binding occurs. To acquire enough DNA to run a small-scale and mid-scale *in vitro* transcription, I used a large-scale PCR reaction protocol which ensured I had 1 mL of 281 µM DNA. The large-scale PCR was carried out with the following amounts:

Table 2:

Volume	**Component**	**Concentration**
870 µL	DEPC Treated water	0.1%
100 µL	PFU buffer	10x
20 µL	dNTPs	10 mM
10 µL	5' Primer	100 mM
10 µL	3' Primer	100 mM
2 µL	Antisense strand	1:100 of a 100 mM stock
5 µL	PFU enzyme	1:25

The components were added in order of the chart above. I ensured the PFU enzyme remained in the freezer until absolutely necessary in order to maintain the integrity of the enzyme. The PFU enzyme was vortexed on high for 15 seconds and the mixture was spun for 30 seconds before the enzyme was added. Once the enzyme was added I split the mixture into 10 PCR tubes with 101 µL in each of them, it is also possible to split the mixture into 8 tubes with 127 µL in each. Once the master mix was split up evenly the amplification parameters were set as follows: 2 minutes at 95°C to denature, 25 cycles of 15 seconds at 95°C, 20 seconds at 51°C,

and 1 minute at 72°C, followed by 10 minutes at 72°C and 4°C to hold at the end of the PCR. This ran for about 1 hour and 20 minutes. Once the PCR was complete, a 3% agarose check gel (1.5 grams agarose with 50 mL 1x TAE buffer, microwaved then 5 µL of ethidium bromide was added) was run to ensure the product of the PCR was the expected size. The RhoBAST aptamer is 60 base pairs. 1 µL of dye was mixed with 5 µL of the DNA from the PCR. The check gel was run at 120 V for 1 hour (time adjusted depending on base pair size). The gel was then imaged under UV light.

In Vitro Transcription

The goal of *in vitro* transcription is to create an RNA copy of our chosen DNA sequence. With the RhoBAST PCR product I produced previously, I set up a small-scale transcription in order to check the quality of the RNA produced and save resources in the case something went awry. Once the small-scale transcriptions were quality checked, a mid-scale transcription was performed. The small-scale and mid-scale transcriptions were carried out with the following amounts:

Table 3:

Small-Scale Volume	**Mid-scale Volume**	**Component**	**Concentration**
77 µL	8.85 mL	DEPC treated water	0.1%
12.5 µL	625 µL	Transcription Buffer	10x
1.5 µL	75 µL	Magnesium Chloride	2M
1 µL	**50 µL**	**DTT**	**1 M**
5 µL each	**250 µL**	**ATP, CTP, GTP, UTP**	**100 mM**
10 µL	**500 µL**	**PCR template**	**280 µM**
2 µL	100 µL	T7 RNA polymerase	*Take out of freezer when ready to put reaction
1 µL	**50 µL**	**IPP**	***Take out of freezer when ready to put in reaction**

****Note:** After the bolded components above, the tube was vortexed on high for 15 seconds and spun.

The components were added in order of the chart above in one tube. Once the reaction was fully mixed, I transferred the tube into a 37°C water bath for 2 hours. Once the reaction was completed, I moved the tube into an ice bucket for immediate use or the -20°C freezer for later use. Polyacrylamide gel electrophoresis (PAGE gel) was run to check the RhoBAST RNA product against a size and intensity marker. The PAGE gel was made as follows:

Table 4:

Volume	**Component**	**Concentration**
30 mL	Diluent	8M Urea & 1x TBE
30 mL	Acrylamide	20% (8M Urea & 1x TBE)
20 µL	TEMED	
200 µL	APS	10%

Before mixing the components, I set the rig up as shown in Figure 9. The Diluent and Acrylamide were mixed first, then TEMED was added, followed by APS. Once the components were added I poured from one corner of the rig to the other, watching for bubbles and leaking. If leaking occurred, I used heated glass bottles of tap water and placed them on top of the glass to speed up the setting process and reduce the amount of leakage. The gel takes around an hour to set but can be expedited by using the same glass bottle technique previously mentioned. Once the gel has had ample time to set (~ 1 hour), the comb used to create the wells and the bottom spacer are removed. The gel is then placed upright on the rig and secured using binder clips. The gel was pre-run for 30 minutes at 13 watts, this ensures the ammonium persulfate is removed before the run occurs. While the gel is pre-running, my samples were prepared by mixing 13 µL of

RNA product with 50 µL of formaldehyde loading dye, then heat-cooling this mixture. Heat-cooling entails placing the dye-RNA mixture in a 95°C heating block for 5 minutes to denature the RNA. After 5 minutes the tube was removed and vortexed on high for 15 seconds followed by spinning and immediately putting the tube into an ice bucket for at least 10 minutes. This will denature any secondary or tertiary structure present. Once the gel had run for 30 minutes, I took 13 µL of the dye-RNA mixture and loaded the gel. I ran the RhoBAST RNA samples for 1.5 hours at 13 watts. Once the run was complete, I removed the gel from the glass placing it in a tub filled with the TBE buffer used in the gel rig. I then placed 10 µL of ethidium bromide in the TBE buffer and mixed well for at least 10 minutes to allow full saturation into the gel. The gel was imaged under UV light.

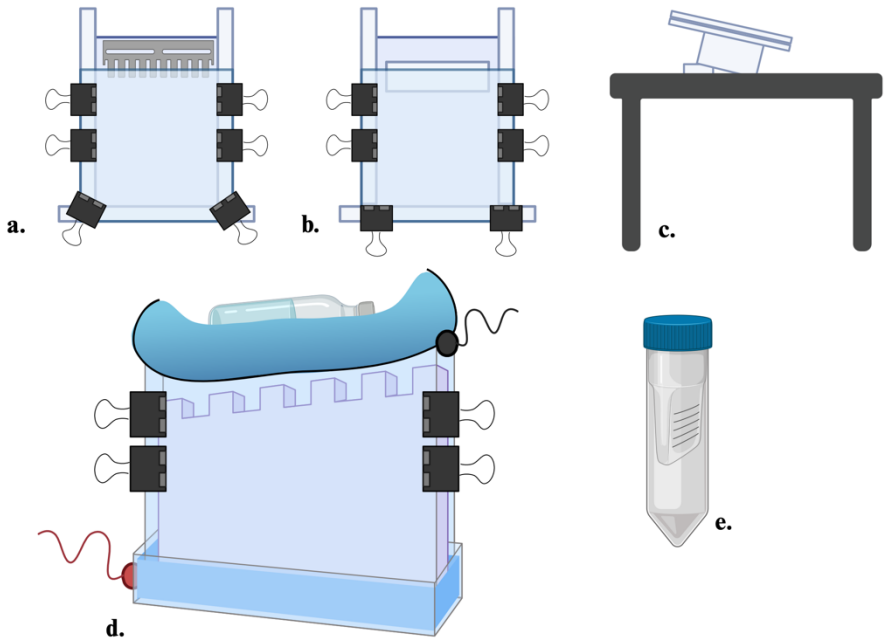

Figure 9: A visual representation of the PAGE gel set up used through the RNA check gel and purification process. (a) Polyacrylamide gel electrophoresis (PAGE) rig set up which was used as a check point to confirm the RNA was the expected size. (b) PAGE RNA purification set up with slight modifications from the check gel itself, including a larger singlet comb and a different placement of binder clips. (c) This figure represents the tilt needed to pour the gel in order to find linkage and prevent the polyacrylamide from leaking. (d) The actual PAGE gel rig with the gel clipped in using binder clips to prevent buffer leakage. There is a water bottle on top to help prevent overuse of the buffer (as long as the buffer is covering the top of the well). The bottom of the gel is covered with TBE buffer as well. (e) This is the 10kDa 50 mL centrifugal filter column used for concentrating and buffer exchanging at the end of RNA purification. Created with BioRender.com.

Gel Purification of RNA

RNA purification ensures the RNA used for future assays is pure allowing for better results. RNA was purified by polyacrylamide gel electrophoresis (PAGE). This is usually done with a large amount of RNA to save resources. In my case this was done with the mid-scale transcription mentioned previously. The PAGE gel is made as follows:

Table 5:

Volume	Component	Concentration
50 mL	Diluent	8M Urea & 1x TBE
50 mL	Acrylamide	20% (8M Urea & 1x TBE)
50 µL	TEMED	
500 µL	APS	10%

The setup for the purification gel is very similar to that of the PAGE check gel, which was explained previously, but using the volumes in the chart above. Additional differences are the spacer sizes and comb size used which are shown in Figure 9. Once the gel is pre-running, I took my mid-scale RNA (~ 6.25 mL) and concentrated that down to ~500 µL at 3200 RPM for 35 minutes in a -10kDa 50 mL centrifugal filter column, so it can be pipetted into the well more efficiently. I then took 500 µL of the RhoBAST RNA and mixed it together with 500 µL of formaldehyde loading dye. Once mixed, I heat-cooled the dye-RNA mixture as previously described and loaded the 1000 µL dye-RNA mixture all at once to ensure even distribution in the well. The gel ran for 2 hours, and 45 minutes based on the position of our dye front at 13 watts. Once the run was complete, the gel was removed from the rig and wrapped in saran wrap to allow for tracing of the RNA to occur. The following steps are done quickly because RNA is

sensitive to UV light. The wrapped gel is placed under UV light. Once the RNA band of interest is located, I traced along the edges of the band with a sharpie. It is important to get as close as you can to the desired band that way there are no other side products retrieved, once complete I removed the gel from the light. I then carefully used a razor blade to cut on the sharpie lines made previously removing the piece from the larger gel. I cut this smaller section of gel into smaller pieces and pushed them through a 10 mL syringe into a 50 mL conical to create a paste with even consistency to allow for maximum extraction of the RNA. The crushed gel was placed in a 50 mL conical that was then filled with DEPC treated water until the 50 mL mark. The tube was placed in the cold room overnight (at least 12 hours) on a rotator to ensure extraction of the RNA.

After extraction, the conical was spun for 15 minutes and the supernatant was transferred to another 50 mL conical. I then refilled the conical containing the pelleted gel with DEPC water until the 50 mL mark and placed it back in the cold room for a second extraction for at least 2 hours.

Once the supernatant was retrieved, the conical was placed on ice, and the RNA in the supernatant was concentrated using a 10x 50 mL column (Figure 9). This took about 3-4 spins depending on the amount of supernatant I had acquired. I aimed to concentrate everything down to 1 mL which took about 25 minutes at 3200 RPM per spin. After concentration, the same column was used for buffer exchange. The column containing the concentrated RNA was filled completely with TE buffer, making sure to pipette up and down to mix. The column was spun until the RNA was concentrated to ~1 mL. This was done a total of three times. Once the third buffer exchange was complete, the RNA was removed and placed in a 1.5 mL Eppendorf tube on ice. A PAGE check gel was run with the acquired RNA to ensure the purification was successful.

Characterizing Fluorescent Dyes

To determine the dye concentration, and fluorescence properties of the JF 549 dyes, absorption, excitation, and emission spectra were collected. For these measurements, a 5 μM stock of JFX 549-HaloTag and JF 549-Alkyne were made in ethanol-TFA. This stock was used for both the excitation and emission spectra on the fluorimeter and the absorbance measurement on the UV-Vis spectrometer. The JF 549-Alkyne and JFX 549-HaloTag excitation spectrum was collected from 500-565 nm while measuring the emission at 585 nm, and the emission spectrum was collected from 560-630 nm while exciting at 540 nm. Another 5 μM stock of each dye was created in an aqueous buffer solution (1x ABS). Once the spectra were collected, these stocks were then diluted into 50 nM, 100 nM, and 500 nM to measure the excitation and emission spectra on a fluorescent plate reader.

Measuring the Interaction Between RNA and Binding Dye

In order to measure dye binding to the RhoBAST aptamer, I relied on fluorescence of the dye. Previous work had shown that when the MaP555 dye bound to RhoBAST, there was an increase in fluorescence. I wanted to use the same principle (a change in fluorescence property) for measuring dye binding. The fluorescence assays were designed as titrations with a known dye concentration and an increasing RNA concentration. A change in fluorescence output (increase or decrease) as a function of RNA concentration was then used to determine the binding affinity. In preparation for the assay, the RNA was Nanodropped, and the concentration was calculated using Beer-Lambert law:

$$\boldsymbol{A = \varepsilon b C}$$

Absorbance (A) or A260 as shown on the Nanodrop, molar absorptivity ($\boldsymbol{\varepsilon}$)**,** the length path of light (b) and finally concentration (C). The stock RNA refers to the originally made and purified

RNA batch that was concentrated to 1 mL and the concentration was calculated to be 837.9 µM. Similarly, the dye concentration for JFX 549-HaloTag and JF 549-Alkyne was determined using the extinction coefficient (101,000$M^{-1}cm^{-1}$) from two separate dye samples in water and ethanol/TFA. Using this approach, I determined the concentration of the stock solutions of JFX 549-HaloTag at 675 µM and JF 549-Alkyne at 130 µM.

To carry out the titration assay, I created a series of RNA dilutions to ensure a wide range of concentrations was achieved. The dilutions were as follows: 400 nM was prepared using 4.8 µL of the stock RNA into 95.2 µL of DEPC. Next, a 40 µM stock was prepared by diluting 9.5 µL of stock RNA with 10.5 µL of DEPC. Next, I prepared a series of dilutions from the 40 µM stock which ranged from 1/10, 1/100, and 1/1000. Once these dilutions were made, they were then heated on a hotplate at 95°C for 5 mins to denature the RNA then placed immediately into ice for a minimum of 10 minutes while the rest of the titration was set up. Next, 15 x 1.5 mL Eppendorf tubes were collected and labeled. It was determined that 15 points (including the background) would be a sufficient number of points for the titration range. Next DEPC treated water was added to each tube. The volume of water (not in buffer) and RNA added up to a total of 15 µL to minimize the pipette switching and overall pipette error. After making the dilutions, and heat-cooling, DEPC treated water was then added never exceeding 15 µL. The buffer-dye-DEPC master mix was then created to ensure a concentration of 10 nM dye for each sample. 10 x ABS buffer and large volumes of water were the consistent throughout. Once the master mix was added, the RNA was taken out of the ice, spun and vortexed. The titration started from lowest RNA concentration to the highest using a p20 and a p10 pipette. Each reaction total was made to 120 µL to plate two technical replicates at 55 µL in each well. Before every well was plated in a 386 Corning FL bottom plate, the Eppendorf tube was vortexed and carefully placed on the side

of the well before pipetting the mixture. It is important to pipette slow and precisely due to the sensitivity of the fluorescent plate reader to focal height. The 16th point plated is the background measurement containing only DEPC and 10x ABS buffer. Once all of the samples are plated, the plate was covered with a lid and left to sit for 1 hour to allow equilibration to occur. After 1 hour the plate was read using a fluorescence plate reader, where gain and focal height were set to the well with the highest amount of RNA to ensure an accurate reading. For the MaP555 dye, the emission was scanned from 575-650 nm upon excitation at 555 nm. The volumes, concentration, and calculations for the master mix (30 reactions) were as follows:

Table 6:

Titration point	RNA concentration (nM)	RNA (stock dilution)	DEPC treated water volume	Master mix volume	Total Eppendorf volume
1	0	0	15	105	120
2	1	3 (1: 1000)	12		
3	5	15 (1: 1000)	0		
4	10	3 (1: 100)	12		
5	50	15 1: 100)	0		
6	100	3 (1: 10)	12		
7	200	6 (1: 10)	9		
8	500	15 (1: 10)	0		
9	1000	3 (40 µM)	12		
10	1500	4.5 (40 µM)	10.5		
11	2000	6 (40 µM)	9		
12	5000	15 (40 µM)	0		
13	10000	3 (400 µM)	12		
14	50000	15 (400 µM)	0		

**15 is only DEPC treated water and 10x ABS buffer **

Below are sample calculations for setting up the titration between MaP555 and RhoBAST RNA.

MaP555 Dye:

$$V = \left[\frac{10\ nm\ (dye\ concentration)}{1\ \mu M\ (dye\ stock\ concentration) * 1000} * 120\ (rxn\ volume)\right] * 30\ rxn$$
$$= 36\ \mu L \text{ of dye per master mix}$$

10x ABS Buffer:

$$V = 12 * 30\ rxn = 360\ \mu L \text{ per master mix}$$

DEPC Water:

$$\left[120(total\ volume) - 15(RNA + water) - 12\ (amount\ of\ buffer) - \left(\frac{36}{30}\right)(dye)\right] * 30\ rxn = 2754\ \mu L \text{ of water per master mix}$$

Volume per well:

$$V = \frac{3150\ (total\ volume\ calculated)}{30\ rxn} = 105\ \mu L \text{ buffer in each reaction}$$

When working with JFX 549-Halotag and JF 549-Alkyne, it was determined the stock concentrations were 675 µM and 130 µM, respectively. These concentrations were obtained from measuring the absorbance of the dyes in water and calculating the concentration from the Beer Lambert law. From here, the previously stated protocol was changed slightly, instead of preparing a 10 nM dye solution for titrations, I prepared a 100 nM solution because this concentration gave me a better signal-to-noise on the fluorescence plate reader (see Results section). The emission spectrum was measured from 571 – 650 nm and upon excitation at 540. Other than the changes above, the samples were prepared as shown in Table 6.

The binding data were fit using the quadratic equation which is as follows:

$$Y = m + (n - m) * (((10 + x + K) - sqrt(sqr(10 + x + K) - (4 * 10 * x)))/(2 * 10))$$

(Y) is the fluorescence value, (m) is the lower asymptote, (n) is the upper asymptote, (x) is the RNA concentration, (K) is the Kd, and (10) is the concentration of the dye. For MaP555 10 nM was used, and for JFX 549-HaloTag and JF 549-Alkyne 100 nM was used. Data fit to this equation produce a Kd value which was used to define the binding affinity.

Results

Overview

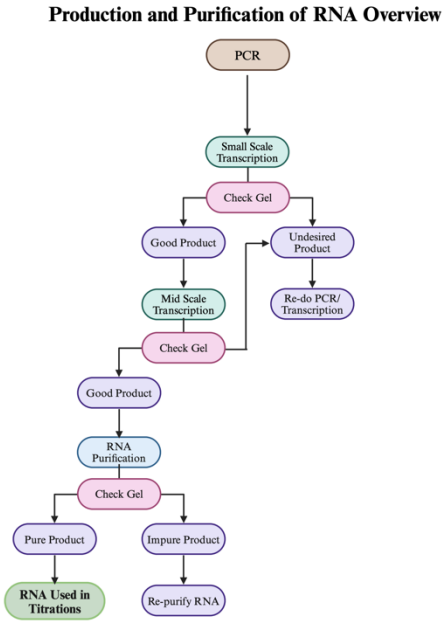

Figure 10: Flow chart of the experimental processes used to obtain a final RNA stock at a high concentration which can be used in titrations to test RNA-dye binding. Created with BioRender.com.

My goal was to examine the interaction between the RhoBAST aptamer and fluorescent dyes, to evaluate these dyes for use in RhoBAST-based biosensors. This required me to synthesize a high yield RhoBAST RNA through *in vitro* transcription. Figure 10 shows a flow chart of my overall workflow for this thesis. First, I used PCR to produce the DNA template for the *in vitro* transcription reaction. Then I carried out a small-scale transcription, testing this on a check gel to ensure I obtained the desired band size and intensity. Once the small-scale transcription was proven successful, I performed a mid-scale transcription. Once mid-scale was proven successful, I purified the RNA. After purification, a final check gel was run. If the gel showed the desired band with little to no outlier bands, then it was used in binding titrations to measure the binding of fluorescent dyes to the RNA aptamer.

Optimizing PCR conditions to produce template DNA

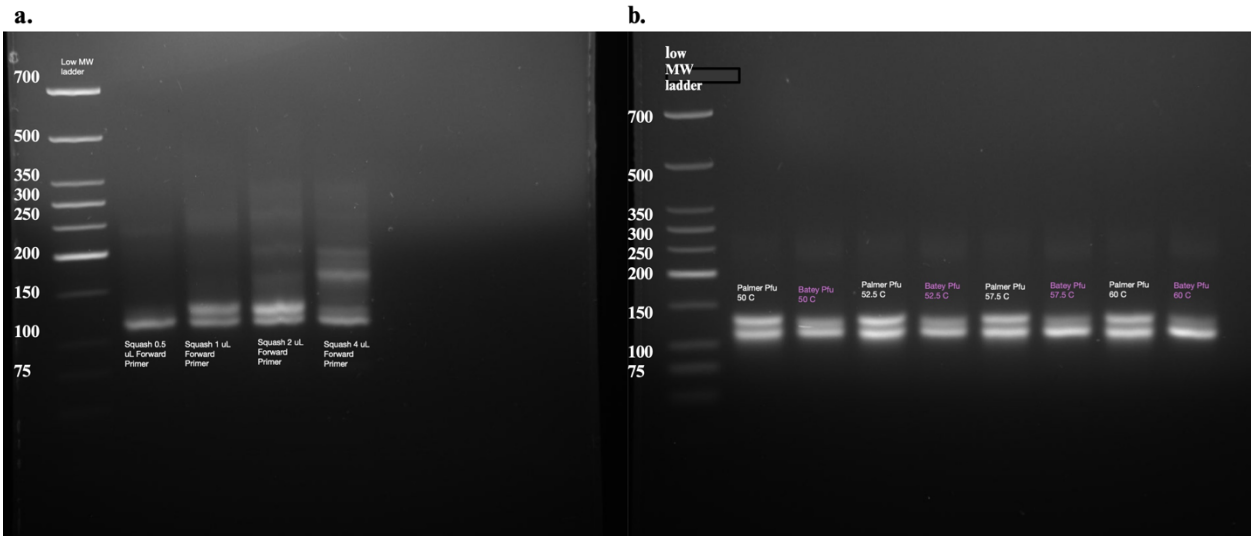

Figure 11: (a) Image of Squash aptamer PCR products on an agarose gel. The labels indicate the primer volume. Also included is a low molecular weight ladder (b) Agarose gel of a temperature gradient ran with the Squash aptamer against a 100 base pair ladder. Each gel was run in a 3% agarose gel conditions at 120v for 1 hour.

I first set out to learn how to carry out PCR and to determine how different reaction conditions affect the production of DNA. In order to check reproducibility of the PCR techniques used, a previously published aptamer Squash was analyzed. Figure 11a represents the optimization of amplification of Squash DNA determined through two experiments. I first carried out a primer gradient which consisted of varying volumes (and hence final concentration) of the forward primer. After this test was conducted, I concluded that there was a DNA yield increase from 0.5 µL to 1 µL and slight increase to 2 µL, which is shown through the increasing intensity of the bands present. Since there was similar yield at volumes of 1 µL and 2 µL, I kept the original protocol of 1 µL for the forward primer. The bottom band present on both agarose gels is the expected band for Squash, which means the top band is likely a result of improper annealing. To help eliminate this top band, the number of PCR cycles was decreased from 25 to 20 since it is a smaller piece of DNA.

Next, I carried out a gradient PCR in which I varied the annealing temperature. Figure 11b shows a temperature gradient from 50 °C to 60 °C using two different sources of Pfu enzyme. There were not many differences in the number and intensity of the bands, but the Palmer lab PFU gave slightly brighter bands (more DNA) than the Batey Lab Pfu enzyme. The temperature also had little effect, but the brightest bands were between 50°C and 52.5°C, which led to the choice of 51°C for the annealing temperature.

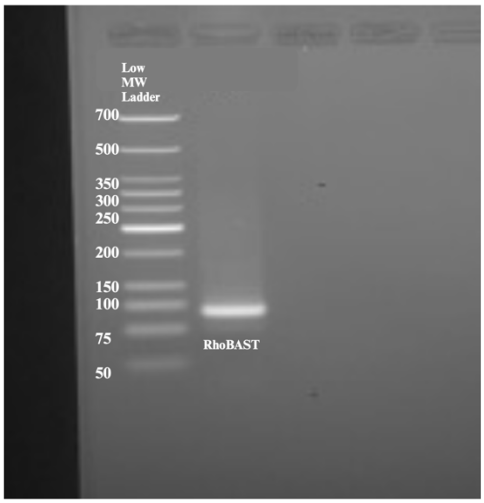

Figure 12: Image of an agarose gel showing the RhoBAST PCR product around the desired size which was reported to be ~75 base pairs (Englert et al., 2023).

Once a PCR protocol was optimized for producing DNA for the Squash aptamer, I carried out PCR to produce a DNA template for RhoBAST. Figure 12 shows an agarose gel of the PCR product. The size is slightly larger than the published size of 75 bp (Englert et al., 2023) because my primers contained a T7 binding site for the in vitro transcription reaction and a G-C clamp.

In Vitro Transcription

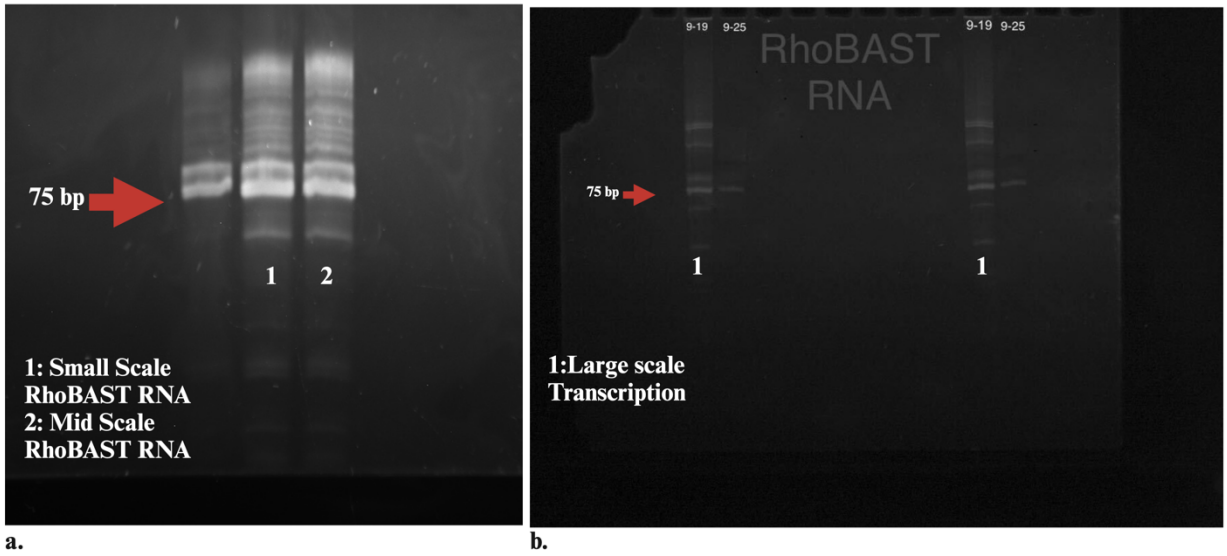

Figure 13: Polyacrylamide gels of products from *in vitro* transcription reactions. (a) Small-scale transcription reaction (~1 mL) (1) compared to a mid-scale transcription (~6.5 mL) (2) of the RhoBAST aptamer RNA. Ignore the first lane which contained an RNA sample from a colleague (b) Shows a large-scale (~12 mL) transcription of RhoBAST RNA. The red arrow is pointing to where ~75 bp sits, which is right below the desired band in both (a) and (b). Created with Biorender.com

After producing template DNA, the next step was to carry out an *in vitro* transcription reaction to make RhoBAST RNA. I tried three different scales of reaction: small, mid-scale, and large. Figure 13 shows polyacrylamide check gels of the products of the *in vitro* transcription reactions. Figure 13a, sample 1 shows the result of the small-scale *in vitro* transcription. The *in vitro* transcription produced the desired product, right above the ~75 bp marker (Figure 13). Other side products were also made in the process. This is a relatively normal occurrence found in *in vitro* transcriptions. The T7 enzyme which controls RNA synthesis and termination can have early termination occur, which leads to smaller sequences of RNA. Longer RNA extensions are made by RNA folding backwards towards the polymerase, allowing more sequence to be added on. This is why we must purify the RNA before using it downstream in fluorescence assays. Figure 13b shows the results of a large-scale transcription of RhoBAST RNA. A large-scale (12 mL) transcription was performed because a large volume of concentrated RNA is

required for the binding assays. While the large-scale shows the desired band size and expected side products, there is a noticeable difference in intensity of the bands when compared to the small-scale transcription; despite being large scale, much less RNA was produced. A mid-scale (6.5 mL) transcription was then run to see if the amount of RNA produced was more or less than that of the large-scale, which would save resources in the long run. Figure 13a shows the results from the mid-scale transcription which has the expected RhoBAST band. The mid-scale transcription produced bands of comparable intensity to the small-scale transcription and higher than the large-scale transcription. Given that the mid-scale transcription produced more RNA than large-scale and produced a comparable concentration but higher volume of RNA than the small-scale transcription, all subsequent *in vitro* transcriptions followed the mid-scale protocol whenever making large amounts of RNA. I also determined that the RNA produced through *in vitro* transcription was sufficient for downstream titrations (Figure 10).

RNA purification

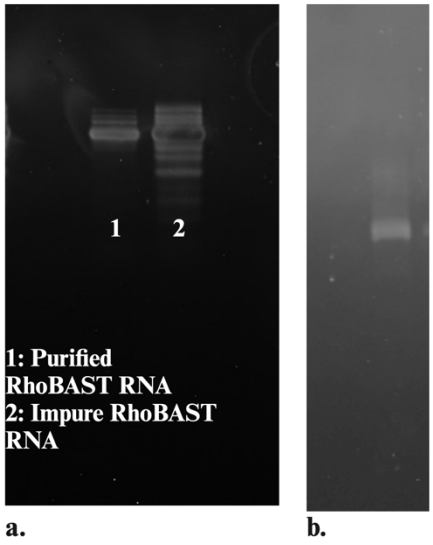

Figure 14: (a) Polyacrylamide check gel comparing pure and impure RhoBAST RNA samples. The RhoBAST RNA was purified twice. The RNA sample in (1) is the final RNA used in RNA-dye titrations. (b) Polyacrylamide check gel showing the unsuccessful first attempt at purification. The RNA contains smeared bands upstream and downstream of the desired band.

While the *in vitro* transcription produced an RNA product the size of RhoBAST, it also produced a lot of other side products that could complicate binding assays. Therefore, purification of RhoBAST RNA was particularly important for downstream binding titrations between RNA and dye. After completion of the first purification process, a check gel was run, and there were still bands present above the desired RNA RhoBAST band indicating purification was not entirely successful (Figure 14b). This most likely occurred due to the formaldehyde loading dye and the RhoBAST RNA running at the same spot on the purification gel, which made it difficult to visualize only the RNA when cutting out the desired band. The purification process was run a second time on the same sample. Running a purification twice would likely lead to product loss, but because I had 36 mL of RNA (~1.2 mM), I predicted I would still have sufficient yield for titration experiments. In order to avoid the same issues that plagued the first purification, the dye was not loaded directly into the RNA but rather was loaded on the side to allow band tracking. Figure 14a shows the result of the second purification. The polyacrylamide gel compares the pure RhoBAST RNA (after two purifications) to impure RNA. When compared to the impure sample, the pure RhoBAST sample had high intensity, but a significant decrease in the number of bands indicating the purification was successful. The concentration of the sample was determined to be 837.9 μM which also proves there was product loss after purification. In order to avoid product loss and time loss by running another purification, this RNA was used in the rest of the titration experiments.

Spectroscopic characterization of the fluorescent dyes

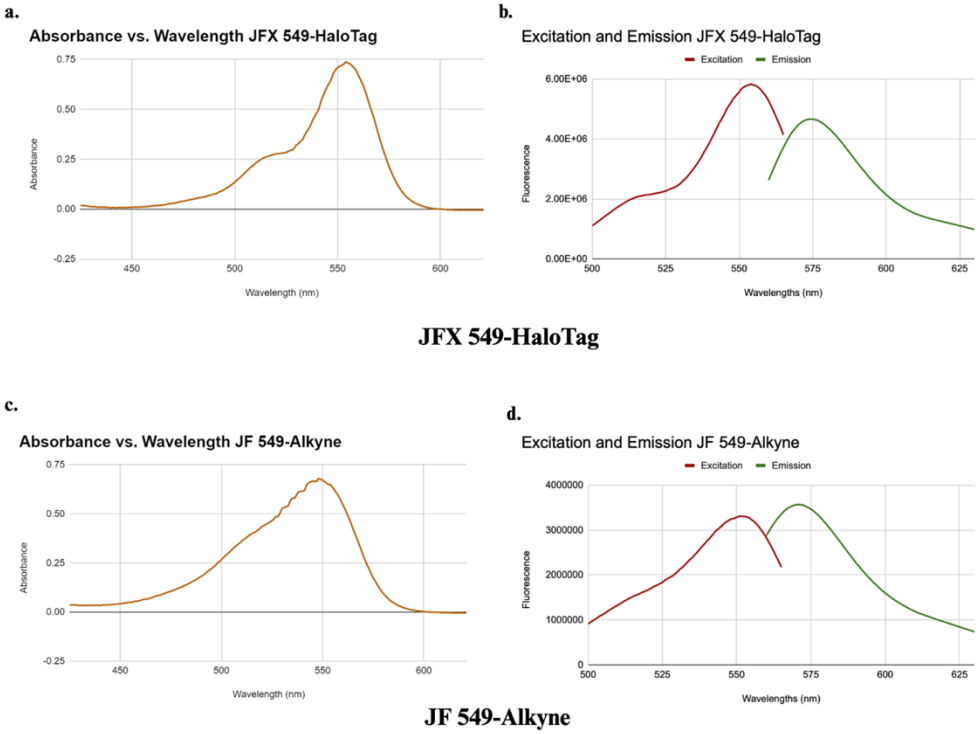

Figure 15: Absorption, excitation, and emission spectra of JF dyes used in this study. (a) An absorbance spectrum of JFX 549-HaloTag in ethanol/TFA. (b) Excitation and emission spectra of JFX 549-HaloTag in ethanol/TFA. Excitation collected from 500-565 emitting at 585. Emission excited at 540 and collected from 560-630. (c) Absorbance spectrum of JF 549-Alkyne in ethanol/TFA. Max abs peak at 554 nm. (d) Excitation and emission spectra of JF 549-Alkyne in ethanol/TFA. Max peak at 548 nm. Excitation collected from 500-565 emitting at 585. Emission excited at 540 and collected from 560-630. Absorbance was collected on a spectrometer and the excitation and emission spectra were collected on a fluorimeter. Created with Biorender.com

Characterizing the dye stocks that are going to be used throughout experiments is important to ensure consistent and accurate data. Figure 15 shows the absorbance, excitation, and emission spectra of a 5 μM solution of JFX 549-HaloTag and JF 549-Alkyne. These are the dyes which are being used in binding experiments with the previously synthesized RNA. Each measurement had the dye prepared in ethanol/TFA as the solvent. Previous studies have shown that this solvent forces the dyes into the open zwitterionic form which increases both absorption and emission (Grimm et al., 2015). Hence the spectrum in ethanol/TFA represent the maximum amount of fluorescence produced by each dye at that particular concentration. These spectra are consistent with previously published literature, confirming the collected excitation and emission

peaks. (Grimm et al., 2018, 2020). This thorough characterization of the dye's concentration and excitation and emission spectra ensure the collection and analysis of future data using these dyes is precise.

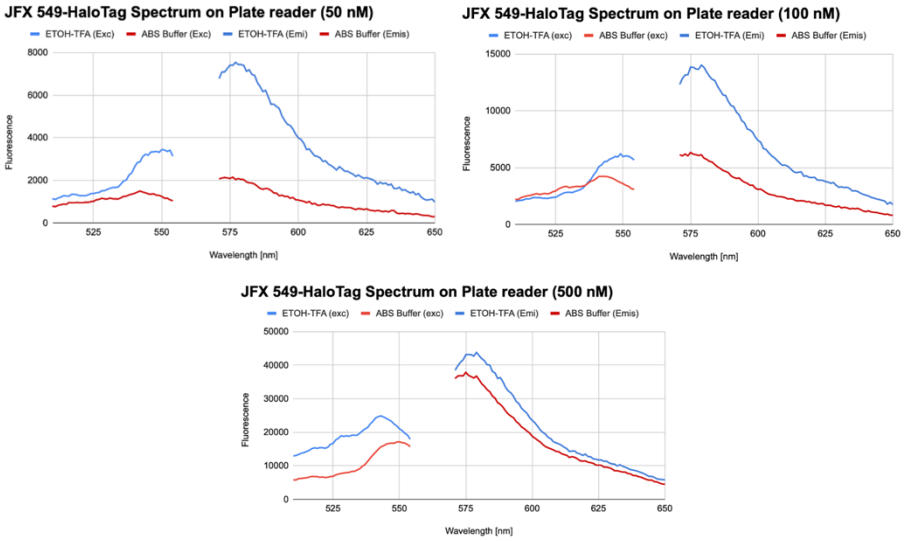

JFX 549-HaloTag

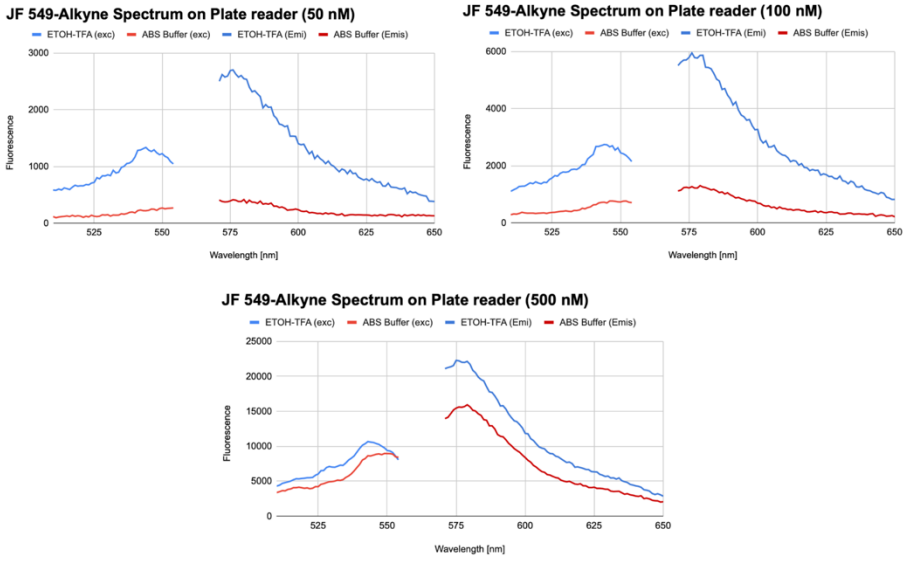

JF 549-Alkyne

Figure 16: Excitation and emission spectra of JFX 549-HaloTag and JF 549-Alkyne at three different concentrations on a fluorescence plate reader. The blue lines represent the dye spectra in ethanol/TFA solvent. The red lines represent the dye spectra in aqueous solution (ABS buffer).

Once I measured spectra on a fluorimeter, it was important to test the sensitivity of the fluorescence plate reader, which I would use for binding experiments. Figure 16 shows the excitation and emission spectra of JFX 549-HaloTag and JF549-alkyne on a fluorescent plate reader. I measured the spectra at three different concentrations to determine the optimal dye concentration for titration assays; I was looking for a concentration that gave rise to a robust spectrum, while also minimizing the amount of dye used. Each dye concentration was also tested in two solvents: aqueous solution (ABS buffer) and ethanol/TFA. This is because the RNA titrations are performed in aqueous solution. The fluorescence produced by JFX 549-HaloTag at each concentration was higher overall versus JF 549-Alkyne in both aqueous solution and ethanol/TFA. This was expected as deuteration of the azetidine ring in JFX led to a higher quantum yield (Grimm et al., 2021). Having two conditions allowed me to test how much the fluorescent signal changed in an aqueous solution vs. an optimal solution where we know the dye behaves best. At all dye concentrations, the signal was higher in ethanol/TFA than the dye in ABS buffer. This suggests that in aqueous solution neither dye is in the fully opened zwitterionic form and raises the possibility that when the dye binds to RNA the fluorescence could in principle increase due to changes in the electrostatic environment around the dye. The fluorescence signal in ethanol/TFA defines the maximum amount of fluorescence the dye can produce. Both JF 549-Alkyne and JFX 549-HaloTag had low signal at 50 nM dye compared to that of 100 nM, particularly for the sample in aqueous buffer. While both dyes showed an impressive signal (2x) at 500 nM dye versus 100 nM, using this high concentration leads to using quite a lot of dye, which didn't seem necessary due to the signal at 100 nM being sufficient. It

was determined that the 100 nM concentration of the dye is the best choice for binding experiments.

Measuring the Interaction Between RNA and Fluorescent Dyes

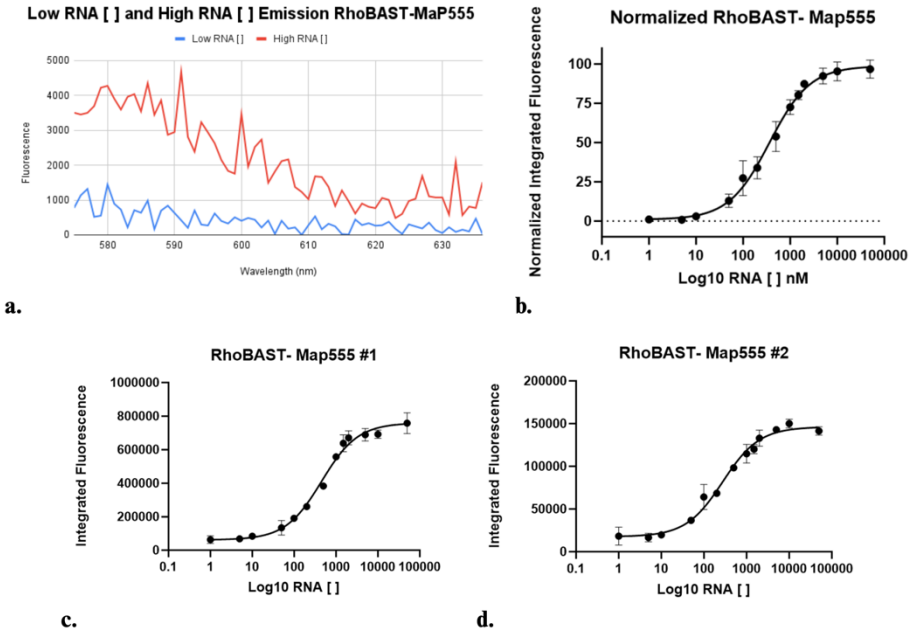

Figure 17: Binding curves for the interaction between RhoBAST and MaP555. (a) 10 nM dye concentration emission spectrum. The line in red is high RNA concentration and the line in blue is low RNA concentration (b) Normalized binding (from 4 replicates) of RhoBAST-Map555 at 10 nM dye concentration. (c) The first biological replicate performed (two technical replicates) of the RhoBAST-Map555 at 10 nM dye concentration starting from low concentration of RNA to high. Kd: 447 $\pm$97 (d) Second biological replicate (two technical replicates) under the same conditions used in (c). Kd: 270 $\pm$ 78.

The overarching objective of my thesis is to discover new dyes that can effectively bind to RhoBAST RNA, potentially enhancing RNA-based biosensors. I plan to utilize the MaP555 dye as a positive control, given its known fluorescence turn-on and established binding affinity regarding the RhoBAST aptamer. Figure 17 shows the change in fluorescence upon binding of MaP555 to RhoBAST. Figure 17a shows that the fluorescence emission of MaP555 increases upon binding to RhoBAST, as shown previously (Englert et al., 2023). To test reproducibility, two technical replicates were performed for each titration, and two biological replicates were performed for a total of 4 replicates. The apparent dissociation constant (Kd) was obtained by fitting the normalized binding curve, as described in the Methods section. The Kd was determined to be 358 nM (± 64). The measured Kd was slightly higher than the Kd measured by other researchers in our lab (~200 nm). These experiments reproduced literature results that MaP555 binds RhoBAST, resulting in a 12-fold change and fluorescence increase. This also validated the RhoBAST RNA that I produced.

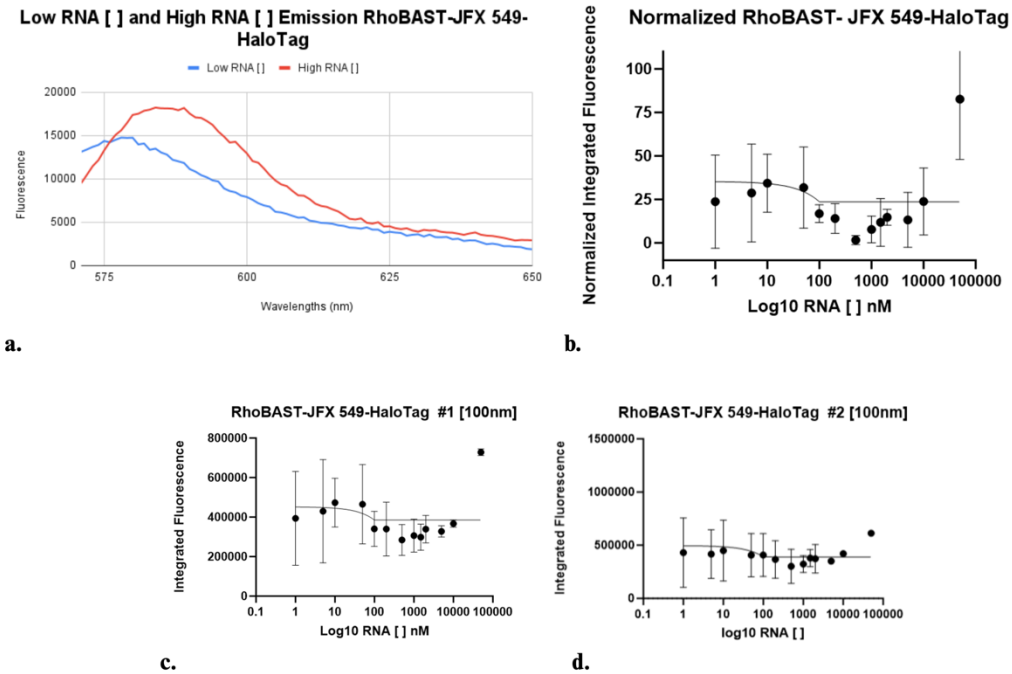

Figure 18: Titration of JFX 549-HaloTag with RhoBAST. (a) 100 nM dye concentration emission spectrum. The line in red is high RNA concentration and the line in blue is low RNA concentration. (b) Normalization of 4

replicates (two overall biological replicates) of RhoBAST-JFX 549-HaloTag in a binding experiment increasing RNA concentrations. (c) The first biological replicate binding titration preformed at 100nM (d) The second replicate experiment using the same conditions as (c).

The next step was to test whether the JFX549-HaloTag and JF549 alkyne could bind RhoBAST and give rise to a change in fluorescence. These dyes differ from Map555 and from each other in a number of ways including differing dye structure and the JF dyes maintain a higher K_{L-Z} . Figure 18 shows the changes in fluorescence upon binding of JFX 549-HaloTag to RhoBAST. The experimental conditions were the same as the RhoBAST-MaP555 experiments, except the dye concentration used was 100 nM. As shown in Figure 18a, there was no change in the emission spectrum of JFX549-HaloTag when low and high RNA concentrations were added. Because there is no change in fluorescence and fluorescence change is used to detect binding, I can't distinguish between JFX549-HaloTag not binding to RhoBAST and JFX549-HaloTag binding, but the binding doesn't change the fluorescence of the dye. When compared to the literature, a previous study found that 5C-JF 549, which contains a carboxylate at the 5' position on the lower ring of the dye, produced a 1.4-fold increase in fluorescence (Englert et al., 2023), which could suggest the much larger chloroalkane tail of JFX 549-Halotag prevents binding, or that binding doesn't alter the equilibrium, perhaps because the dye is already more shifted toward the open zwitterionic form.

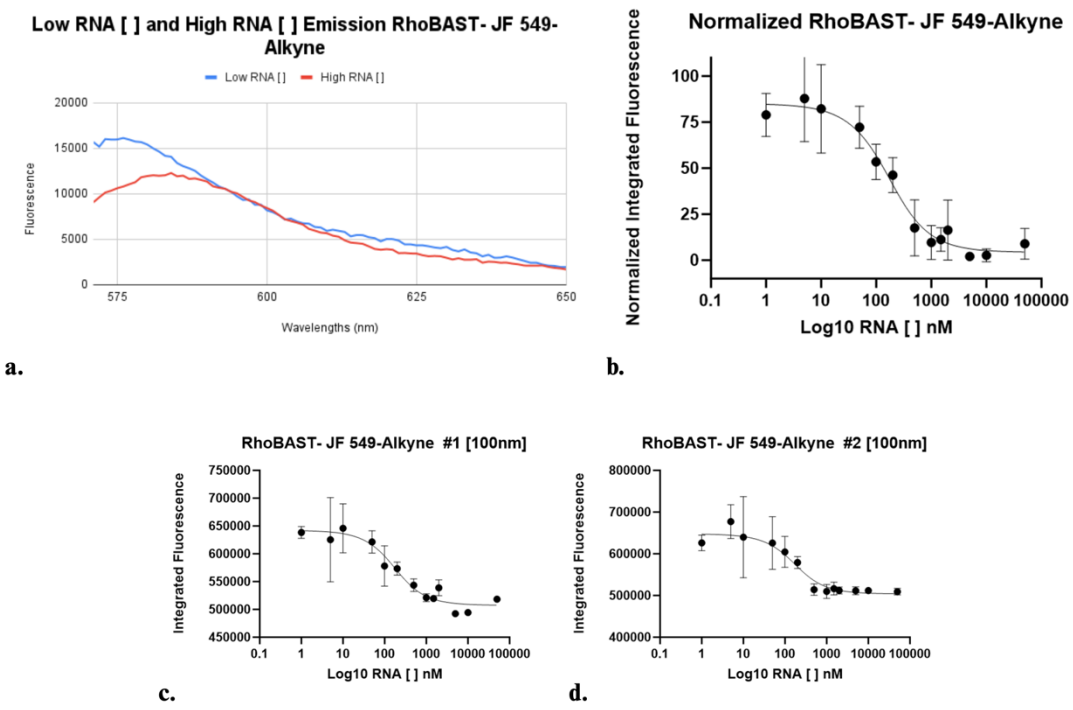

Figure 19: Changes in fluorescence upon binding of JF549-Alkyne to RhoBAST. (a) 100 nM dye concentration emission spectrum. The line in red is high RNA concentration and the line in blue is low RNA concentration (b) Normalized integrated fluorescence change of 4 replicates (two overall biological replicates) upon titration of JF 549-Alkyne with increasing RhoBAST RNA. (c) Integrated fluorescence intensity of the first biological replicate binding titration preformed at 100 nM. Kd: 124 ± 159 (d) Integrated fluorescence intensity of the second replicate experiment using the same conditions as (c). Kd: 120 ±154.

The next dye I sought to test was JF549-alkyne. JF549-alkyne contains an alkyne moiety off the 6' position of the bottom ring in the fluorophore. Figure 19 shows the titration of JF 549-alkyne with RhoBAST RNA. The experimental conditions were the same as the RhoBAST-MaP555 experiments, except the dye concentration used was 100 nM. As the RNA concentration was increased, the fluorescent signal decreased, as shown by measuring the bottom and top point of the titration in Figure 19a. This result ultimately suggests that when JF 549-Alkyne binds with the RNA, the dye's fluorescence signal is quenched, converting more of the dye into its closed lactone form. The Kd was determined by fitting the normalized binding curve (Figure 19b) to the

quadratic formula (refer to methods), and the Kd was found to be 121.9 nM (± 76) showing a relatively high binding affinity between RhoBAST and the dye.

Discussion

The overarching goal of my thesis was to test a broader repertoire of rhodamine-based dyes to determine if they could bind the RhoBAST aptamer and if binding altered the fluorescence properties. My hypothesis was that because rhodamine-based dyes exist in an equilibrium between a closed, non-fluorescent lactone form and an open, fluorescent zwitterionic form, and because the position of this equilibrium depends on the local chemical environment, that binding to RNA could shift the equilibrium and cause a change in fluorescence. Previous research has indicated that when these dyes bind to proteins (such as HaloTag) or RNA (as evidenced by MaP555's interaction with RhoBAST), it results in changes to their chemical environment leading to increased fluorescence. This suggests that binding to proteins or RNA may influence the equilibrium towards the open or zwitterionic form. However, it is important to acknowledge that this effect may vary among different dyes due to their unique initial K_{L-Z} value.

The binding experiments performed between RhoBAST and JFX 549-HaloTag showed that there was no overall change in fluorescence as the dye was titrated with increasing concentrations of RNA. Because there was no change in fluorescence, I can't say whether or not the JF dye and RhoBAST RNA bind. It could also be that binding doesn't change the K_{L-Z} equilibrium because the chemical environment of the RNA doesn't favor one form over the other. To test binding, I would need to use a different method for measuring the association between the dye and the RNA. For example, I could use techniques such as Isothermal Titration Calorimetry (ITC) or SHAPE analysis which can detect the interaction between a small molecule and an RNA without requiring a change in fluorescence.

The binding experiment between RhoBAST and JF 549-Alkyne showed that the fluorescence signal decreased as the dye was titrated with increasing concentrations of RNA. This suggests that binding of the dye to the RNA favors the closed non-fluorescent lactone form of the fluorophore. While the fluorescence signal decreases upon binding, the Kd of 124 nM was comparable to the Kd of MaP555 binding to RhoBAST (~ 200 nM).

The differences in chemical composition between JFX 549-HaloTag, JF 549-Alkyne, and MaP555 offer valuable insight into the effects of dye binding to RNA. As shown in Figure 20, the notable differences in the chemical structure of these dyes are the following: 1) MaP555 has two methyl groups coming off of each N on the xanthene core, while both JF549 dyes have azetidine rings at this same position, 2) when MaP555 is in the open form, it has an acyl-sulfamide group, whereas both JF549 dyes have a carboxylic acid, 3) both the JF dyes have a functional group off the 6' position of the lower ring, whereas MaP555 doesn't have any additional moieties. While the equilibrium between the closed spiro-cyclic form and open zwitterion is not fully understood, researchers try to shift the equilibrium to the closed form by adding electron withdrawing groups (such as fluorine) to the xanthene ring (Wang et al., 2020) or by adding electron withdrawing groups to destabilize the spirolactam (as in the case of MaP555) (Wang et al., 2020). The azetidine rings were initially added to tetramethyl rhodamine in place of the two methyl groups to increase the quantum yield. While this made for a very bright fluorophore, it also is the case that JF549 has a high $K_{L\text{-}Z}$ and hence is primarily in the open zwitterionic form. The electron withdrawing group in the spirolactam of MaP555 favor the closed form, which gives MaP555 more opportunity to "turn on" than the JF549 dyes. JF 549-Alkyne has a smaller K_{L-Z} than JFX 549-Halotag. With a lower K_{L-Z} comes greater potential to modulate the fluorescence intensity, even if that means a decrease in fluorescence signal upon

binding RNA. This may be why JF549-alkyne shows a change in fluorescence upon binding RhoBAST, while JFX549-HaloTag doesn't. This structural difference gives less opportunity for static-collision or dynamic collisions which in turn is why this dye does not quench the RNA, but instead the fluorescence increases as it binds.

Both JFX 549-HaloTag and JF 549 Alkyne have something bound to the 6th position as shown in Figure 20, but showed different results when RNA was added. It is unlikely that this structural difference (HaloTag vs Alkyne) has an effect on the binding of RNA or is the reason for quenching of the fluorescent signal when binding. In order to determine this to be true, a test on the same dye set containing a change only in the 6th position needs to be conducted to really narrow down whether or not these structures truly have an effect on RNA binding. The difference in fluorescence upon binding RNA between the JF549-Alkyne and JF549-HaloTag is more likely due to the deuterium that was added in place of the hydrogens on JFX 549-HaloTag. Deuterium is known to have an effect on the quantum yield, such that JFX 549-HaloTag has a higher quantum yield (Grimm et al., 2021). As noted above, JFX 549 has a higher K_{L-Z} equilibrium which suggests that the zwitterionic form is highly favored and there is less opportunity to modulate fluorescence by shifting the equilibrium. This could explain why no change in fluorescence signal was produced as RNA concentration increased. This suggests the deuterium may increase the K_{L-Z}. Similarly to the previous suggestion, testing the JF 549 dyes with only deuterium present or not with the same 6th position could narrow down how this affects the JF 549 dye.

The structural differences between the three dyes also provide some valuable insight into the binding properties of RhoBAST. Interestingly, the bulky azetidine rings on JF549-Alkyne don't hinder binding to RhoBAST. In fact, in my hands, JF549-Alkyne binds slight better than

MaP555 which has less bulky methyl groups off the nitrogen. This suggests that the RhoBAST RNA can accommodate more chemical bulk off the xanthene ring.

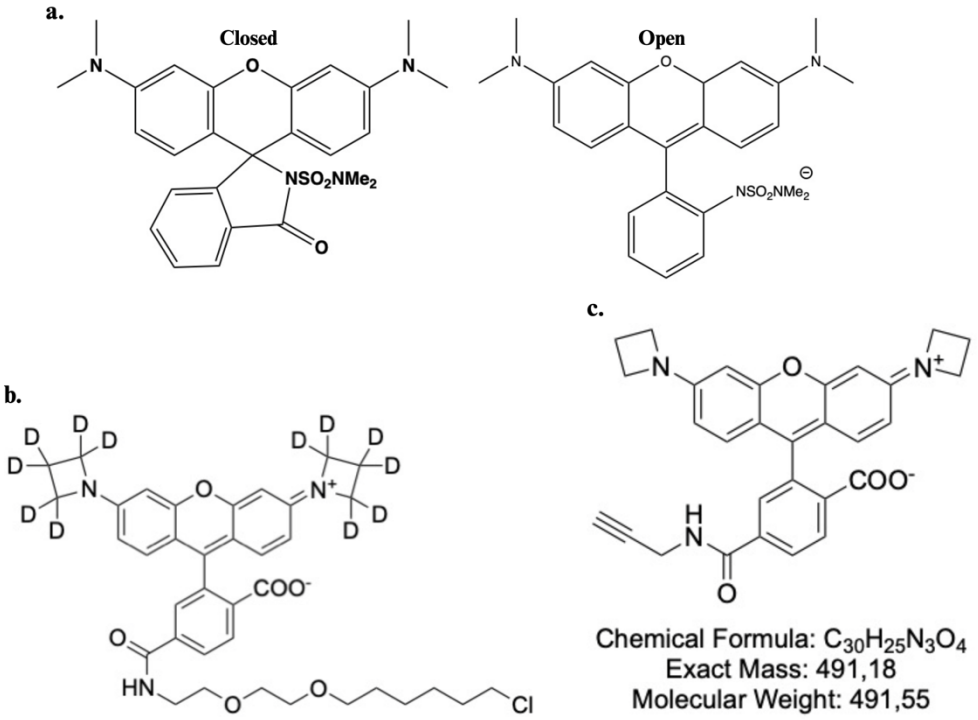

Figure 20: (a) Structural representation of the MaP555 fluorescent dye in open and closed form. (b) Structural representation of JFX 549-HaloTag. (c) Structural representation of JF 549-Alkyne. Created with Biorender.com

Finally, my ultimate goal was to determine whether either JFX549-HaloTag or JF549-Alkyne might be suitable dyes to use with RhoBAST instead of MaP555. From the data I have collected, JFX 549-HaloTag would not be a strong dye for RhoBAST due to the lack of fluorescence change upon binding the RNA. JF549-Alkyne showed some potential in that the fluorescence changed upon binding and the Kd demonstrated that the binding affinity was strong. However, it is generally preferable in biosensors for the fluorescence signal to increase rather than decrease. So, where do we go from here? In an attempt to find new dyes that would effectively show an increase in fluorescence signal when RNA is added, I would go for a set of dyes that rely on the opening of the lactone ring which means they have a smaller K_{L-Z} values.

This would allow more room for fluorescence increase instead of always being on at almost the peak fluorescence signal. I don't believe structural modifications like the difference in the 6th position on the JF549 dyes have a large effect on the fluorescence, but additives near the three aromatic rings could (tetramethyl versus azetidine rings). Additionally, electron withdrawing groups in the spirolactam moiety may influence the propensity of the dye to turn on upon binding. So, I would want to look at a variety of JF dyes and MaP dyes that incorporate the above differences. There are many ways to engineer a fluorophore, and narrowing down which ways give us the best fluorescence signal and bind effectively will lead to a robust dye library for the RhoBAST aptamer.

Conclusion

In conclusion, dyes with similar structures like JFX 549-HaloTag and JF 549 Alkyne can lead to vastly different fluorescence signals when bound to the RhoBAST RNA. While these dyes are highly regarded for their bright and photostable fluorescence, differences in the on-and-off equilibrium can occur. While the JF 549-Alkyne does have a lower K_{L-Z} , the shift itself occurs differently than other reported dyes with similar equilibriums. In order to fully understand how each dye will interact with the RNA it is important to look at the whole picture. Paying attention to the chemical environment for fluorescence turn-on is crucial to understanding the binding that is occurring between the RNA and the dye. Also having an understanding for which aqueous solvents are optimal for a set of dyes that can also be used cellularly is an avenue worth taking. Shedding light on how the RNA itself interacts with the dyes can give a lot of information on how the structure of the dye effects binding, so assessing binding autonomous of the fluorescence turn-on is valuable. Lastly, it can be important to characterize dyes which absorb at the same wavelength but are structurally different similar (similar to the experiments conducted here), and structurally the same dyes at different wavelengths to see if the spectra of these dyes effects that of which fluorescence occurs.

In summary, while this study sheds light on the behaviors of RhoBAST RNA with JF 549 dyes containing structural differences, further investigation is necessary to fully elucidate the nature of these interactions and their implications for metabolite tracking.

Acknowledgments

I would like to express my sincere gratitude to the entire Palmer lab for being so open and willing to deal with three extremely energetic undergraduate researchers at once, when I am sure one of us was enough to deal with. I would also like to thank the Batey lab for teaching me everything I know about RNA (even though it barely scratches the surface) and allowing me and my fellow researchers to consume all of your knowledge and techniques. I extend my wholehearted thanks to Logan McCoy and Aleksandra Weirzba for who I owe the entirety of my project too, because without them this thesis may have just been an essay. Thank you for teaching me and allowing me to grow. Lastly, A special thank you to Dr. Amy Palmer my PI who inspires me in every way, not only to be a strong and ethical researcher, but to educate passionately and believe I can do anything and whatever happens, it will be okay.

I am extremely grateful for the opportunity to be an undergraduate researcher. I would also like to thank the BSI scholarship for funding my first summer as a researcher.

I would like to thank my family and friends for supporting me in my crazy ways, for without them I would not be the person I am today.

References

Baird, N. J., Kulshina, N., & Ferré D'Amaré, A. R. (2010). Riboswitch function: Flipping the switch or tuning the dimmer? *RNA Biology*, *7*(3), 328–332. https://doi.org/10.4161/rna.7.3.11932

Bajar, B., Wang, E., Zhang, S., Lin, M., & Chu, J. (2016). A Guide to Fluorescent Protein FRET Pairs. *Sensors*, *16*(9), 1488. https://doi.org/10.3390/s16091488

Bhalla, N., Jolly, P., Formisano, N., & Estrela, P. (2016). Introduction to biosensors. *Essays in Biochemistry*, *60*(1), 1–8. https://doi.org/10.1042/EBC20150001

Clark, L. C., & Lyons, C. (1962). ELECTRODE SYSTEMS FOR CONTINUOUS MONITORING IN CARDIOVASCULAR SURGERY. *Annals of the New York Academy of Sciences*, *102*(1), 29–45. https://doi.org/10.1111/j.1749-6632.1962.tb13623.x

Dey, S. K., Filonov, G. S., Olarerin-George, A. O., Jackson, B. T., Finley, L. W. S., & Jaffrey, S. R. (2022). Repurposing an adenine riboswitch into a fluorogenic imaging and sensing tag. *Nature Chemical Biology*, *18*(2), 180–190. https://doi.org/10.1038/s41589-021-00925-0

Englert, D., Burger, E.-M., Grün, F., Verma, M. S., Lackner, J., Lampe, M., Bühler, B., Schokolowski, J., Nienhaus, G. U., Jäschke, A., & Sunbul, M. (2023). Fast-exchanging spirocyclic rhodamine probes for aptamer-based super-resolution RNA imaging. *Nature Communications*, *14*(1), 3879. https://doi.org/10.1038/s41467-023-39611-1

Greenwald, E. C., Mehta, S., & Zhang, J. (2018). Genetically Encoded Fluorescent Biosensors Illuminate the Spatiotemporal Regulation of Signaling Networks. *Chemical Reviews*, *118*(24), 11707–11794. https://doi.org/10.1021/acs.chemrev.8b00333

Grimm, J. B., English, B. P., Chen, J., Slaughter, J. P., Zhang, Z., Revyakin, A., Patel, R., Macklin, J. J., Normanno, D., Singer, R. H., Lionnet, T., & Lavis, L. D. (2015). A general method to improve fluorophores for live-cell and single-molecule microscopy. *Nature Methods*, *12*(3), 244–250. https://doi.org/10.1038/nmeth.3256

Grimm, J. B., Muthusamy, A. K., Liang, Y., Brown, T. A., Lemon, W. C., Patel, R., Lu, R., Macklin, J. J., Keller, P. J., Ji, N., & Lavis, L. D. (2018). *A general method to fine-tune fluorophores for live-cell and in vivo imaging*.

Grimm, J. B., Tkachuk, A. N., Xie, L., Choi, H., Mohar, B., Falco, N., Schaefer, K., Patel, R., Zheng, Q., Liu, Z., Lippincott-Schwartz, J., Brown, T. A., & Lavis, L. D. (2020). A general method to optimize and functionalize red-shifted rhodamine dyes. *Nature Methods*, *17*(8), 815–821. https://doi.org/10.1038/s41592-020-0909-6

Grimm, J. B., Xie, L., Casler, J. C., Patel, R., Tkachuk, A. N., Falco, N., Choi, H., Lippincott-Schwartz, J., Brown, T. A., Glick, B. S., Liu, Z., & Lavis, L. D. (2021). A General Method to Improve Fluorophores Using Deuterated Auxochromes. *JACS Au*, *1*(5), 690–696. https://doi.org/10.1021/jacsau.1c00006

Herman, B. (1998). Fluorescence Microscopy. *Current Protocols in Cell Biology*, *00*(1). https://doi.org/10.1002/0471143030.cb0402s13

Leamy, K. A., Yennawar, N. H., & Bevilacqua, P. C. (2017). Cooperative RNA Folding under Cellular Conditions Arises From Both Tertiary Structure Stabilization and Secondary Structure Destabilization. *Biochemistry*, *56*(27), 3422–3433. https://doi.org/10.1021/acs.biochem.7b00325

Lichtman, J. W., & Conchello, J.-A. (2005). Fluorescence microscopy. *Nature Methods*, *2*(12), 910–919. https://doi.org/10.1038/nmeth817

Martynov, V. I., Pakhomov, A. A., Popova, N. V., Deyev, I. E., & Petrenko, A. G. (2016). Synthetic Fluorophores for Visualizing Biomolecules in Living Systems. *Acta Naturae*, *8*(4), 33–46. https://doi.org/10.32607/20758251-2016-8-4-33-46

McDaniel, B. A. M., Grundy, F. J., Artsimovitch, I., & Henkin, T. M. (2003). Transcription termination control of the S box system: Direct measurement of *S* -adenosylmethionine by the leader RNA. *Proceedings of the National Academy of Sciences*, *100*(6), 3083–3088. https://doi.org/10.1073/pnas.0630422100

Ovechkina, V. S., Zakian, S. M., Medvedev, S. P., & Valetdinova, K. R. (2021). Genetically Encoded Fluorescent Biosensors for Biomedical Applications. *Biomedicines*, *9*(11), 1528. https://doi.org/10.3390/biomedicines9111528

Paige, J. S., Nguyen-Duc, T., Song, W., & Jaffrey, S. R. (2012). Fluorescence Imaging of Cellular Metabolites with RNA. *Science*, *335*(6073), 1194–1194. https://doi.org/10.1126/science.1218298

Sahil, M., Singh, J., Sahu, S., Pal, S. K., Yadav, A., Anand, R., & Mondal, J. (2023). Identifying Selectivity Filters in Protein Biosensor for Ligand Screening. *JACS Au*, *3*(10), 2800–2812. https://doi.org/10.1021/jacsau.3c00374

Sunbul, M., Lackner, J., Martin, A., Englert, D., Hacene, B., Grün, F., Nienhaus, K., Nienhaus, G. U., & Jäschke, A. (2021). Super-resolution RNA imaging using a rhodamine-binding aptamer with fast exchange kinetics. *Nature Biotechnology*, *39*(6), 686–690. https://doi.org/10.1038/s41587-020-00794-3

Sunbul, M., Lackner, J., Martin, A., Englert, D., Hacene, B., Nienhaus, K., Nienhaus, G. U., & Jäschke, A. (2020). *RhoBAST - a rhodamine-binding aptamer for super-resolution RNA imaging* [Preprint]. Cell Biology. https://doi.org/10.1101/2020.03.12.988782

Tsien R. Y. (1998). The green fluorescent protein. *Annual review of biochemistry*, *67*, 509–544. https://doi.org/10.1146/annurev.biochem.67.1.509

Wang D, Farhana A. Biochemistry, RNA Structure. [Updated 2023 Jul 29]. In: StatPearls [Internet]. Treasure Island (FL): StatPearls Publishing; 2024 Jan-. Available from: https://www.ncbi.nlm.nih.gov/books/NBK558999/#

Wang, L., Tran, M., D'Este, E., Roberti, J., Koch, B., Xue, L., & Johnsson, K. (2020). A general strategy to develop cell permeable and fluorogenic probes for multicolour nanoscopy. *Nature Chemistry*, *12*(2), 165–172. https://doi.org/10.1038/s41557-019-0371-1

Zheng, Q., Ayala, A. X., Chung, I., Weigel, A. V., Ranjan, A., Falco, N., Grimm, J. B., Tkachuk, A. N., Wu, C., Lippincott-Schwartz, J., Singer, R. H., & Lavis, L. D. (2019). Rational Design of

Fluorogenic and Spontaneously Blinking Labels for Super-Resolution Imaging. *ACS Central Science*, *5*(9), 1602–1613. https://doi.org/10.1021/acscentsci.9b00676